Hydrol. Earth Syst. Sci. Discuss., https://doi.org/10.5194/hess-2017-454
Manuscript under review for journal Hydrol. Earth Syst. Sci.
Discussion started: 28 August 2017

Hydrology and Earth System Sciences
Discussions

Assessment of actual evapotranspiration over a semi-arid heterogeneous land surface by means of coupled low resolution remote sensing data with energy balance model: comparison to extra Large Aperture Scintillometer measurements

Sameh Saadi[1,2], Gilles Boulet[1], Malik Bahir[1], Aurore Brut[1], Bernard Mougenot[1], Pascal Fanise[1], Vincent Simonneaux[1], and Zohra Lili Chabaane[2]

[1]Centre d'Etudes Spatiales de la Biosphère, Université de Toulouse, CNRS, CNES, IRD, UPS, Toulouse, France

[2] Université de Carthage / Institut National Agronomique de Tunisie/ LR17AGR01-GREEN-TEAM, Tunis, Tunisie;

Correspondence to: Sameh Saadi (saadi_sameh@hotmail.fr)

Abstract.

In semi-arid areas, agricultural production is restricted by water availability; hence efficient agricultural water management is a major issue. The design of tools providing regional estimates of evapotranspiration (ET), one of the most relevant water balance fluxes, may help the sustainable management of water resources.
Remote sensing provides periodic data about actual vegetation temporal dynamics (through the Normalized Difference Vegetation Index NDVI) and water availability under water stress (through the land surface temperature LST) which are crucial factors controlling ET.
In this study, spatially distributed estimates of ET (or its energy equivalent, the latent heat fluxes LE) in the Kairouan plain (Central Tunisia) were computed by applying the Soil Plant Atmosphere and Remote Sensing Evapotraspiration (SPARSE) model fed by low resolution remote sensing data (Terra and Aqua MODIS). The work goal was to assess the operational use of the SPARSE model and the accuracy of the modelled i) sensible heat flux (H) and ii) daily ET over a heterogeneous semi-arid landscape with a complex land cover (i.e. trees, winter cereals, summer vegetables).
The SPARSE's layer approach was run to compute instantaneous estimates of H and LE fluxes at the satellite overpass time. The good correspondence (R^2= 0.60 and 0.63 and RMSE=57.89 W/m^{-2} and 53.85 W/m^{-2}; for Terra and Aqua, respectively) between instantaneous H estimates and large aperture scintillometer (XLAS)'s H measurements along a pathlength of 4 km over the study area showed that the SPARSE model presents satisfactory accuracy. Results showed that, despite the fairly large scatter, the instantaneous LE can be suitably estimated at large scale (RMSE=47.20 W/m^{-2} and 43.20 W/m^{-2}; for Terra and Aqua, respectively and R^2= 0.55 for both satellites). Additionally, water stress was investigated by comparing modelled (SPARSE derived) to observed (XLAS derived) water stress values; we found that most points were located within a 0.2 confidence interval, thus the general tendencies are well reproduced. . Even though extrapolation of instantaneous latent heat flux values to daily totals was less obvious, daily ET estimates are deemed acceptable.

KEYWORDS: Evapotranspiration, Remote sensing, SPARSE model, scintillometer, water stress.

1 Introduction

In water scarce regions, especially arid and semi-arid areas, the sustainable use of water by resource conservation as well as the use of appropriate technologies to do so is a priority for agriculture (Amri et al., 2014; Pereira et al., 2002).

Water use rationalization is needed especially for countries actually suffering from water scarcity, or for countries that probably would suffer from water restrictions according to climate change scenarios. This implies that closely monitoring the water budget components is a major issue (Oki and Kanae, 2006).

The estimation of evapotranspiration (ET) is of paramount importance since it represents the preponderant component of the terrestrial water balance; it is the second greatest component after precipitation (Glenn et al., 2007); hence ET quantification is a key factor for scarce water resources management. Direct measurement of ET is only possible at local scale (single plot) using the eddy-covariance method for example; whereas, it is much more difficult at larger scales (irrigated perimeter or watershed) due to the complexity of hydrological processes (Minacapilli and Ciraolo, 2007). Moreover, at these scales, land cover is usually heterogeneous and this affects the land-atmosphere exchanges of heat, water and other constituents (Giorgi and Avissar, 1997). ET estimates for various temporal and spatial scales, from hourly to monthly to seasonal time steps, and from field to global scales, are required for hydrologic applications in water resource management (Anderson et al., 2011). Techniques using remote sensing (RS) information are therefore essential when dealing with processes that cannot be represented by point measurements only (Su, 2002).

In fact, the contribution of RS in vegetation's physical properties monitoring on large areas have been identified for years (Tucker, 1978); RS provides periodic data about some major ET drivers, amongst others, land surface temperature and vegetation properties (e.g. Normalized Difference Vegetation Index NDVI and Leaf Area Index LAI) from plot to regional scales (Li et al., 2009; Mauser and Schädlich, 1998). Many methods using remotely-sensed data to estimate ET are reviewed in Courault et al.(2005).Water and energy exchange in the soil-plant-atmosphere continuum have been simulated through several land surface models (Bastiaanssen et al., 2007; Feddes et al., 1978). Among them, two different approaches use remote sensing data to estimate spatially distributed ET (Minacapilli et al., 2009): one based on the soil water balance (SWB) and on that solves the surface energy budget (SEB). The SWB approach exploits only visible-near-infrared (VIS-NIR) observations to perceive the spatial variability of crop parameters. The SEB modelling approach uses visible (VIS), near-infrared (NIR) and thermal (TIR) data to solve the SEB equation by forcing remotely-sensed estimates of the SEB components (mainly the land surface temperature LST). In fact, there is a strong link between water availability in the soil and surface temperature under water stress, hence, in order to estimate soil moisture status as well as actual ET at relevant space and timescales, information in the TIR domain (3–15 µm) is frequently used (Boulet et al., 2007). The SWB approach has the advantage of high resolution and frequency VIS-NIR remote sensing data availability against limited availability of high resolution thermal imagery for the SEB approach. Indeed, satellite data such as Landsat or Advanced Spaceborne Thermal Emission and Reflection Radiometer (ASTER) provide accurate field scale (30–100 m) estimates of ET (Allen et al., 2011), but they have a low temporal resolution (16 day-monthly) (Anderson et al., 2011).

The RS-based SWB models provide estimation of ET, soil water content, and irrigation requirements in a continuous way. For instance, at plot scale, accurate estimates of seasonal ET and irrigation can be obtained by

SWB modeling using high resolution remote sensing forcing as done in the study with the SAtellite Monitoring of IRrigation (SAMIR) model by Saadi et al.(2015) over the Kairouan plain. However, for an appropriate estimation of ET, the SWB model requires knowledge of the water inputs (precipitation and irrigation) and an assessment of the extractable water from the soil (mostly derived from, say, actual water content in the root zone, wilting point and field capacity), whereas, significant bias are found mainly when dealing with large areas and long periods, due to the spatial variability of the water inputs uncertainties as well as the inaccuracy in estimating other flux components such as the deep drainage (Calera et al., 2017). Hence, the major limitation of the SWB method is the high number of needed inputs whose estimations are likely uncertain especially over a heterogeneous land surface due to hydrologic processes complexity. Moreover, spatially distributed SWB models (typically those using the FAO guidelines (Allen et al., 1998) for crop ET estimation) generally parameterize the vegetation characteristics on the basis of land use maps (Bounoua et al., 2015; Xie et al., 2008), and different parameters are used for different land use classes. Nevertheless, SWB modelers generally do not have the possibility to carry out remote sensing-based land use change mapping due to time, budget, or capacity constraints and use often very generic classes potentially leading to modeling errors (Hunink et al., 2017). In addition, the lack of data about the soil properties (controlling field capacity, wilting point and the water retention) as well as the actual root depths for heterogeneous areas crops, lead to limited practical use of the SWB models (Calera et al., 2017). The same apply to the soil evaporation whose estimation generally rely on the FAO guidelines approach (Allen et al., 1998). Although, it was shown that under high evaporation conditions, the FAO-56 daily evaporation computed on the basis of the readily evaporable water (REW) is overestimated at the beginning of the dry down (Mutziger et al., 2005; Torres and Calera, 2010). Hence, to improve its estimation a reduction factor proposed by Torres and Calera (2010) was applied to deal with this problem in several studies (e.g. Odi-Lara et al., 2016; Saadi et al., 2015). Furthermore, since actual ET is computed based on actual soil moisture status, the limited knowledge of the actual farmers' irrigation scheduling is a further critical limitation for SWB modeling. Therefore, SWB modelers must deal with the lack of information about real irrigation which induces unreliable estimations. Consequently, ET estimation at regional scale is often achieved using SEB approaches, by combining surface temperature from medium to low resolution (kilometer scale) remote sensing data with vegetation parameters and meteorological variables (Liou and Kar, 2014). Recently, many efforts have been made to feed remotely sensed surface temperature into ET modelling platforms in combination with other critical variables, e.g., NDVI and albedo (Kalma et al., 2008; Kustas and Anderson, 2009). A wide range of satellite-based ET models were developed, and these methods are reviewed in Liou and Kar (2014). The majority of SEB-based models are "single-source models"; their algorithms compute a total latent heat flux as the sum of the evaporation and the transpiration components using a remotely sensed surface temperature. However, separate estimates of evaporation and transpiration makes the "dual-source models" more useful for agrohydrological applications (water stress detection, irrigation monitoring etc.) (Boulet et al., 2015).

Contrarily to SWB models, most SEB models are run in their most standardized version, using observed remote sensing-based parameters such as albedo in conjunction with a set of input parameters taken from literature or *in situ* data. On the other hand, the SEB model validation with enough data in space and time is difficult to achieve, due to the limited availability of high resolution thermal images (Chirouze et al., 2014). Therefore, it is usually possible to evaluate SEB models results only at similar scale (km) to medium or low resolution images. Indeed, the pixel size of thermal remote sensing images, except for the scarce Landsat7 images (60 m), covers a range of

1000 m (Moderate Sensors Resolution Imaging Spectroradiometer MODIS), to the order of 4000 m (Geostationary Operational Environmental Satellite GOES). However, direct methods measuring sensible heat fluxes (eddy covariance EC for example) only provide point measurements with a footprint considerably smaller than a satellite pixel (except for Landsat). Therefore, scintillometry techniques have emerged as one of the best tools aiming to quantify averaged fluxes over heterogeneous land surfaces (Brunsell et al., 2011). They provide average sensible heat estimates over areas comparable to those observed by satellites (Hemakumara et al., 2003; Lagouarde et al., 2002b). Scintillometry can provide sensible heat using different wavelengths, aperture sizes and configurations (Meijninger et al., 2002). The upwind area contributing the flux (i.e. the flux footprint) varies as wind direction and atmospheric stability , and must be estimated for the surface measurements in order to compare them to SEB estimates of the flux which are representative of the pixel (Brunsell et al., 2011). Assessing the upwind area contributing to the flux can be done using several footprint models (Schmid, 2002). The LAS technique has been validated over heterogeneous landscapes against EC measurements (Bai et al., 2009; Chehbouni et al., 2000; Ezzahar et al., 2009) and also against modelled fluxes (Marx et al., 2008; Samain et al., 2012; Watts et al., 2000). Few studies dealt with extra large aperture scintillometer (XLAS) data (Kohsiek et al., 2006; Kohsiek et al., 2002; Moene et al., 2006). Historical survey, theoretical background as well as recent works in applied research concerning scintillometry are reviewed in De Bruin and Wang (2017). Since the scintillometer only provides spatially averaged sensible heat flux (H_XLAS), the latent heat flux (LE_XLAS) can then be computed as the energy balance residual term (LE_XLAS =Rn-G-H_XLAS), hence, the estimation of a representative value for the available energy (AE =Rn-G) is always crucial for the accuracy of the retrieved values of LE_XLAS.

In this study, spatially distributed estimates of surface energy fluxes (sensible heat H and latent heat fluxes LE) over an irrigated area located in the Kairouan plain (Central Tunisia) were obtained by the SEB method, using the “layer” approach (a resistance network that relates the soil and vegetation heat sources to a main reference level using a series electrical branching) of the Soil Plant Atmosphere and Remote Sensing Evapotraspiration (SPARSE) model (Boulet et al., 2015) fed by 1-km thermal data and 1-km NDVI data from MODIS sensors on Terra and Aqua satellites.

The main objective of this paper is to compare H and LE obtained using the SPARSE model and XLAS measurements acquired during two years over a large, heterogeneous area. We explore the consistency between the instantaneous H and LE estimates at the satellite overpass time, the water stress estimates and also ET derived at daily time step from both approaches.

2 Experimental site and datasets

2.1 Study area

The study site is a semi-arid region located in central Tunisia, the Kairouan plain (9°23′−10°17′E, 35°1′−35°55′N, (Figure 1). The landscape is mainly flat, and the vegetation is dominated by agricultural production (cereals, olive groves, fruit trees, market gardens, Zribi et al., 2011). Water management in the study area is typical of semi-arid regions with an upstream sub-catchment that transfers surface and subsurface flows collected by a dam (the El Haouareb dam), and a downstream plain (Kairouan plain) supporting irrigated agriculture (Figure 1). Agriculture consumes more than 80% of the total amount of water extracted each year from the Kairouan aquifer (Poussin et al., 2008). Most farmers in the plain uses their own wells to extract water for irrigation (Pradeleix et al., 2015), while a few depends on public irrigation schemes based on collective networks of water distribution pipelines all linked to a main borehole. The crop intensification in the last decades, associated to increasing irrigation, has led to growing water demand, and an overexploitation of the groundwater (Leduc et al., 2004).

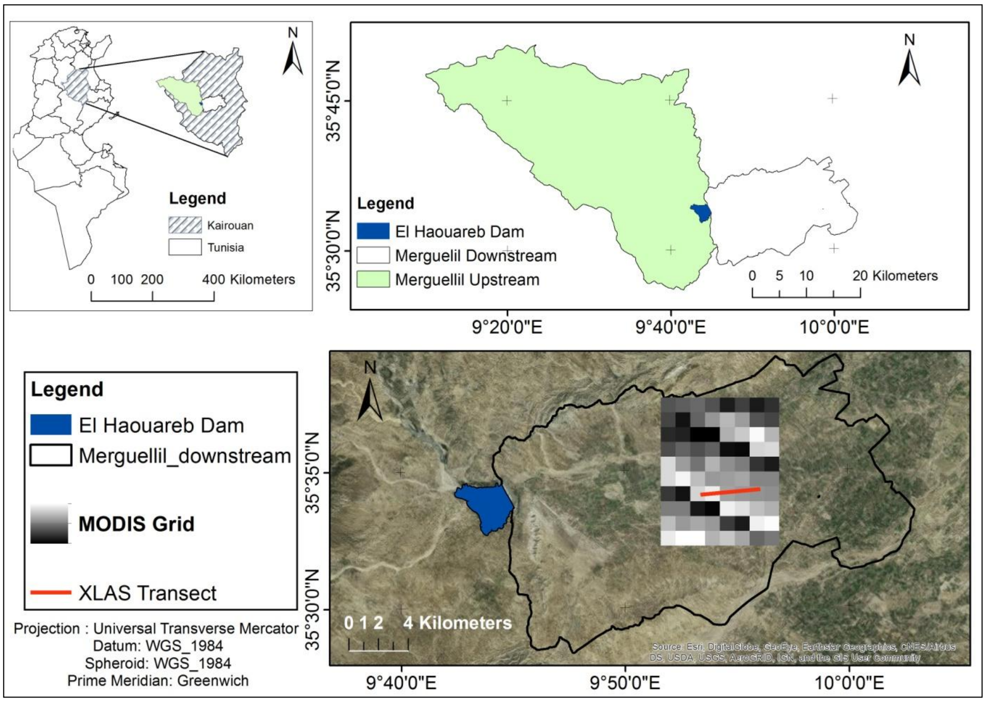

Figure 1 : The study area: the downstream Merguellil sub-basin is the so called Kairouan plain; MODIS grid is the extracted 10 km× 8 km MODIS sub-image

2.2 Experimental Setup

An optical Kipp and Zonen Extra Large Aperture Scintillometer (XLAS) was operated continuously for more than two years (1 March 2013 to 3 June 2015) over a relatively flat terrain. The scintillometer consists in a double device, with a transmitter and a receiver both with an aperture diameter of 0.3 m. The wavelength of the light beam emitted by the transmitter is 940 nm. The transmitter was located on the eastern water tower (coordinates: 35° 34' 0.7" N; 9° 53' 25.19" E) and the receiver on the western water tower (coordinates: 35° 34' 17.22" N; 9° 56' 7.30"E) separated by a path length of 4 km (Figure 2). Both instruments were installed at 20 m height. The scintillometer transect was above mixed vegetation canopy: trees (mainly olive orchards) with some annual crops (cereals and market gardening).

Furthermore, two similar eddy covariance (EC) systems were also positioned at the same level on the two water tower top platforms. Half hourly sensible heat flux, wind speed components and wind direction were measured used a sonic anemometer CSAT 3D at a rate of 20 Hz and a sonic anemometer RM81000 at a rate of 10 Hz, respectively. These EC set-ups (friction velocity u_* and wind direction measurements) were used to compute scintillometer derived fluxes as well as footprints. Half hourly standard meteorological measurements including global incoming radiation, wind speed, air temperature and humidity, rainfall were recorded using an automated weather station installed in the study area (Figure 2). Hereafter, this weather station is referred as the Ben Salem meteorological station (35° 33' 1.44" N; 9° 55' 18.11"E).

In addition, a flux station based on the eddy correlation method, referred as the Ben Salem flux station (few tens of meters away from the meteorological station) was installed from November 2012 to June 2013 in an irrigated wheat field. This station measuring continuously LE was used to perform the extrapolation of instantaneous energy balance components at daily time scale.

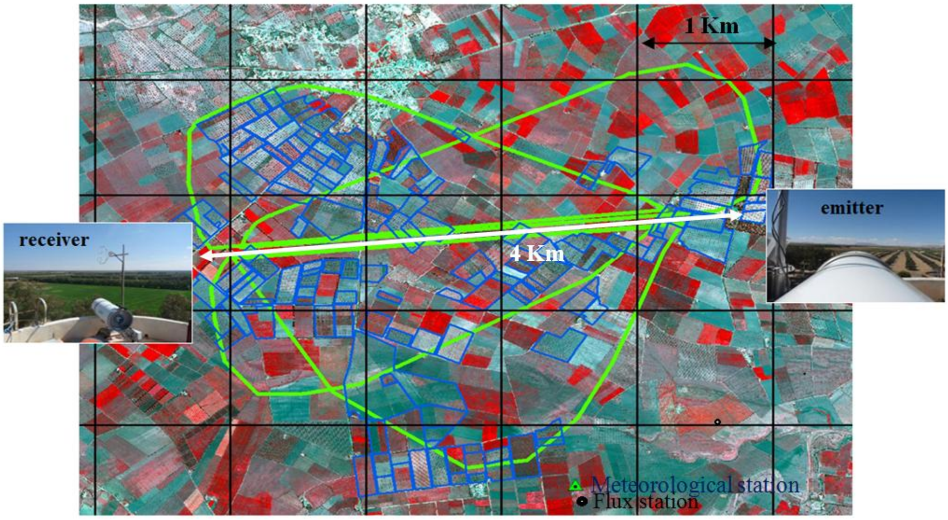

Figure 2 : XLAS Set-up (XLAS transect (white), emitter and receiver locations and half-hourly footprint in typical wind conditions (green), MODIS grid (black), trees plots (blue) and the location of the meteorological and the wheat field flux station. This figure illustrates three colour (red, green, blue) composite of SPOT5 bands 3, 2 and 1.

3 Extra Large aperture scintillometer: data processing

3.1 Scintillometer derived fluxes

Scintillometer is based on the scintillation method. Fluxes of sensible heat and momentum cause atmospheric turbulence close to the ground, and creates, with surface evaporation, refractive index fluctuations due mainly to air temperature and humidity fluctuations (Hill et al., 1980). The fluctuations intensity is directly linked to sensible and latent heat fluxes.

The light beam emitted by the XLAS transmitter towards the receiver is dispersed by the atmospheric turbulence. The scintillations representing the intensity fluctuations are analyzed at the XLAS receiver and are expressed as the structure parameter of the refractive index of air integrated along the optical path C_{n^2} [m$^{-2/3}$] (Lagouarde et al., 2002a; Wang et al., 1978). The sensitivity of the scintillometer to C_{n^2} along the bean is not uniform and follows a bell-shape curve. As transmitter and receiver apertures are equal, the curve is symmetrical. As a result the scintillometer is more sensitive to turbulences, hence to fluxes, in the middle of its path.

In order to compute the XLAS sensible heat flux , C_n^2 was converted to the structure parameter of temperature C_T^2 [K^2 m$^{-2/3}$] by introducing the Bowen ratio (ratio between sensible and latent heat fluxes), hereafter referred to as β, which is a temperature /humidity correlation factor. Moreover, the height of scintillometer beam above the surface varies along the path. Consequently, $C_n^{\,2}$ and therefore $C_T^{\,2}$ are not only averaged horizontally but vertically as well.

At visible wavelengths, the refractive index is more sensitive to temperature than humidity fluctuations Then, we can relate the C_{n^2} to C_{T^2} :

$$C_{n^2} \approx \left(\frac{-0.78 \times 10^{-6} \times P}{T^2}\right)^2 C_{T^2} \left(1 + \frac{0.03}{\beta}\right)^2 \tag{1}$$

with T is the air temperature (°K) and P is the atmospheric pressure (Pa).

Green and Hayashi(1998) proposed another method to compute the sensible heat flux (H) assuming full energy budget closure and using an iterative process without the need of the Bowen ratio as an input parameter. This method is called the "β-closure method" (BCM, Solignac et al., 2009;Twine et al., 2000). Then, the similarity relationship proposed by (Andreas, 1988) is used to relate the C_{T^2} to the temperature scale T_* in unstable atmospheric conditions:

$$\frac{C_{T^2}\,(z_{LAS} - d)^{\frac{2}{3}}}{T_*^2} = 4.9 \times \left(1 - 6.1 \times \left(\frac{z_{LAS} - d}{L_O}\right)^{-\frac{2}{3}}\right) \tag{2}$$

and for stable atmospheric conditions:

$$\frac{C_{T^2}\,(z_{LAS} - d)^{\frac{2}{3}}}{T_*^2} = 4.9 \times \left(1 + 2.2 \times \left(\frac{z_{LAS} - d}{L_O}\right)^{\frac{2}{3}}\right) \tag{3}$$

where L_O (m) is the Obukhov length , Z_{LAS} (m) is the scintillometer effective height, and d (m) is the displacement height, which corresponds to 2/3 of the averaged vegetation height z_v (see Sect. 4.1).

From T_* and the friction velocity, u_* , the sensible heat flux can be derived as follows:

$$H = -\rho c_p T_* u_* \tag{4}$$

where ρ (kg m^{-3}) is the density of air and c_p (J Kg^{-1} K^{-1}) is the specific heat of air at constant pressure.

XLAS sensible heat flux (H_XLAS) was computed at a half hourly time step. Negative night-time data were set to zero and daytime flux missing data (one to three 30mn- data) were gap filled using simple interpolation. Flux anomalies in early morning (circa sunrise) and late afternoon (circa sunset) were corrected on the basis of the ratio between sensible heat flux and half hourly incoming solar radiation measurements (Rg) using Ben Salem meteo station. Furthermore, aberrant values of XLAS sensible heat flux were ruled out.

3.2 XLAS footprint computation

The footprint of a flux measurement defines the spatial context of the measurement and the source area that influences the sensors. In case of inhomogeneous surfaces like patches of various land covers and moisture variability due to irrigation, the measured signal is dependent on the fraction of the surface having the strongest influence on the sensor and thus on the footprint size and location. Footprint models (Horst and Weil, 1992; Leclerc and Thurtell, 1990) have been developed to determine what area is contributing the heat fluxes to the sensors as well as the relative weight of each particular cell inside the footprint limits. Contributions of upwind locations to the measured flux depend on the height of the vegetation, height of the instrumentation, wind speed, wind direction, and atmospheric stability conditions (Chávez et al., 2005).

According to the model of (Horst and Weil, 1992), for one-point measurement system, the footprint function *f* relates the spatial distribution of surface fluxes, $F_0(x,y)$ *to* the measured flux at height z_m, $F(x,y,z_m)$, as follows:

$$F(x,y,z_m) = \int_{-\infty}^{\infty}\int_{-\infty}^{x} F_0(x',y')f(x-x',y-y',z_m)dx'dy' \tag{5}$$

The footprint function *f* is computed as:

$$\bar{f}^y(x,z_m) \cong \frac{d\bar{z}}{dx}\frac{z_m}{\bar{z}^2}\frac{\bar{u}(z_m)}{\bar{u}(c\bar{z})}Ae^{-(z_m/b\bar{z})^r} \tag{6}$$

Where $\bar{u}(z)$ is the mean wind speed profile and $\bar{z}$ is the mean plume height for diffusion from a surface source. The variables *A*, *b* and *c* are scale factors and r a scale factor of the Gamma function. In the case of a scintillometer measurement, the footprint function has to be combined with the spatial weighting function *W(x)* of the scintillometer to account for the sensor integration along its path. Thus, the sensible heat flux footprint mainly depends on the scintillometer effective height z_{LAS} (Hartogensis et al., 2003), which includes the topography below the path and the transmitter and receiver heights, the wind direction and the Obukhov length L_O, which characterizes the atmospheric stability (Solignac et al., 2009).

In a subsequent step, daily footprints were computed based on the half hourly footprints.

3.3 XLAS derived latent heat flux

Instantaneous ($LE\_residual\_XLAS_{t\text{-}FP}$) and daily ($LE\_residual\_XLAS_{day\text{-}FP}$) XLAS derived latent heat flux (i.e residual latent heat flux) of the XLAS upwind area were computed using the energy budget closure of the XLAS measured sensible heat flux (H_XLAS) with additional estimations of net surface radiation Rn combined with soil heat flux G, as available energy (AE=Rn-G), as follows:

$$\mathrm{LE\_residual\_XLAS_{t-FP}} = \mathrm{AE_{t-FP}} - \mathrm{H\_XLAS_t} \tag{7}$$

$$\mathrm{LE\_residual\_XLAS_{day-FP}} = \mathrm{AE_{day-FP}} - \mathrm{H\_XLAS_{day}} \tag{8}$$

H_XLAS_t is the scintillometer sensible heat flux at the time of the satellite overpass interpolated from the half hourly fluxes measurements. Daily H (H_XLAS_{day}) was computed as the average of the half hourly XLAS-measured H. Daily available energy ($AE_{day\text{-}FP}$) was computed from instantaneous available energy ($AE_{t\text{-}FP}$) as detailed in Sect. 3.3.1 and Sect. 3.3.2.

3.3.1 Instantaneous available energy

Net surface radiation is the balance of energy between incoming and outgoing shortwave and longwave radiation fluxes at the land-atmosphere interface. Remote sensed surface radiative budget components provide unparalleled spatial and temporal information, thus several studies have attempted to estimate net radiation by combining remote sensing observations with surface and atmospheric data. Net radiation equation can be written as follows:

$$\mathrm{Rn} = (1-\alpha)\mathrm{Rg} + \varepsilon_s \times \mathrm{R_{atm}} - \varepsilon_s * \sigma * \mathrm{LST}^4 \tag{9}$$

where Rg is the incoming shortwave radiation (W.m^{-2}), R_{atm} is the incoming longwave radiation (W.m^{-2}), ε_s is surface emissivity, σ is Stefan-Boltzmann coefficient (W.m^{-2}.K^{4}) , α is albedo, and LST is land-surface temperature (°K).

The soil heat flux G depends on the soil type and water content as well as the vegetation type (Allen et al., 2005).The direct estimation of G by remote sensing data is not possible (Allen et al., 2011), however, empirical relations could estimate the fraction G/Rn as a function of soil and vegetation characteristics using satellite image data, such as the LAI, NDVI, α and LST. In order to estimate the G/Rn ratio, several methods have been tested for various types of surfaces at different locations (Bastiaanssen, 1995; Burba et al., 1999; Choudhury et al., 1987; Jackson et al., 1987; Kustas and Daughtry, 1990; Kustas et al., 1993; Ma et al., 2002; Payero et al., 2001).

Danelichen et al.(2014) evaluated the parameterization of these different models in three sites in Mato Grosso state in Brazil and found that the model proposed by Bastiaanssen (2005) showed the best performance for all sites, followed by the model from Choudhury et al. (1987) and Jackson et al. (1987). Hence to estimate G, we tested three methods:

Bastiaanssen (2005) :

$$\mathrm{G = Rn \times (LST - 273.16) \times (0.0038 + 0.0074\alpha) \times (1 - 0.98NDVI^4)} \quad (10)$$

Choudhury et al. (1987):

$$G = Rn \times 0.4 \times (\exp(-0.5LAI)) \quad (11)$$

Jackson et al. (1987)

$$G = Rn \times 0.583 \times (\exp(-2.13NDVI)) \quad (12)$$

Remote sensing variables α, LST, ε_s, LAI and NDVI were calculated at the resolution of the sensor (MODIS, 1 km resolution). The Ben Salem meteo station was used to provide Rg and R_{atm}. MODIS Available Energy AE_t was computed for a 10 km × 8 km sub-image centered on the XLAS transect at Terra-MODIS and Aqua-MODIS overpass time, using the three methods estimating G. Since, the measured heat fluxes H_XLAS_t represents only the weighted contribution of the fluxes from the upwind area to the tower (footprint) then instantaneous footprint at the time of Terra and Aqua overpass were selected among the two half hour preceding and following the satellite's time of overpass (lowest time interval) and then was multiplied by AE_t to get the available energy of the upwind area $AE_{t\text{-}FP}$.

3.3.2 Daily available energy

Most methods using TIR domain data rely on once-a-day acquisitions, late morning (such as Terra-MODIS overpass time) or early afternoon (such as Aqua-MODIS overpass time). Thus, they provide a single instantaneous estimate of energy budget components, since the diurnal cycle of the energy budget is not recorded. In order to obtain daily AE from these instantaneous measurements (Eq. (13) and Eq. (14)) and to reconstruct hourly variations of AE, we considered that its evolution was proportional to another variable whose diurnal evolution can be easily known. Here the global solar incoming radiation Rg was used to scale AE from instantaneous to daily values as follows:

$$\mathrm{AE_{day_{Terra}} = a_{Terra} \times Rg_{day} \frac{AE_{t_{Terra}}}{Rg_t} + b_{Terra}} \quad (13)$$

$$\mathrm{AE_{day_{Aqua}} = a_{Aqua} \times Rg_{day} \frac{AE_{t_{Aqua}}}{Rg_t} + b_{Aqua}} \quad (14)$$

where Rg_t and Rg_{day} are respectively the instantaneous and daily global incoming solar radiation.

A bias was found when assuming $a_{Terra}=a_{Aqua}=1$ and $b_{Terra}=b_{Aqua}=0$; hence basing on the Ben Salem flux station Rn and G measurements, corrected parameterizations of AE (a and b) were computed and used to remove this bias (see Sect. 6.1). Consequently, daily available energy was computed for the 10 km × 8 km sub-image at the time of Terra-MODIS ($\mathrm{AE_{day_{Terra}}}$) and Aqua-MODIS ($\mathrm{AE_{day_{Aqua}}}$) overpass, and then was weighted by the corresponding daily footprint to get the daily available energy of the upwind area $AE_{day\text{-}FP}$.

Finally, estimates of Terra-MODIS and Aqua-MODIS observed daily LE were obtained based on the three methods used to compute the soil heat flux G.

4 SPARSE model

4.1 Energy fluxes derived from SPARSE model

The SPARSE model solves the energy budgets of the soil and the vegetation. Main unknowns are the component temperatures, i.e. the temperature of the soil (T_s) and that of the vegetation (T_v). Totals at the reference height, as well as the longwave radiation budget, are also solved so that altogether a system of five equations can be built:

$$\begin{cases} H = H_s + H_v \\ LE = LE_s + LE_v \\ R_{ns} = G + H_s + LE_s \\ R_{nv} = H_v + LE_v \\ \sigma T_{rad}^4 = R_{atm} - R_{as} - R_{av} \end{cases} \tag{15}$$

R_{atm} is the atmospheric radiation (W/m^{-2}), Ra is the net component longwave radiation (W/m^{-2}) and T_{rad} is the radiative surface temperature (°K) as observed by the satellite; indexes “s” and “v” designate the soil and the vegetation, respectively.

The first two (Eq. (15)) express the continuity of the latent and sensible heat fluxes from the sources to the aerodynamic level through to the reference level, the third and the fourth (Eq. (15)) are the soil and vegetation energy budgets, and the fifth (Eq. (15)) relates the radiative surface temperature T_{rad} to T_s and T_v.

The SPARSE model system of equations is fully described in Boulet et al.(2015). SPARSE is similar to the TSEB model (Kustas and Norman, 1999) but includes classical expressions of the aerodynamic resistances (Choudhury and Monteith, 1988;Shuttleworth and Gurney, 1990) .

System (15) is solved iteratively by following similar guidelines as in the TSEB model: the first step assumes that the vegetation transpiration is maximum, and evaporation is computed. If this soil latent heat flux (LE_s) is negative, the hypothesis that the vegetation is unstressed is no longer valid. In that case, the vegetation is assumed to suffer from water stress and the soil surface is assumed to be already long dry. Then, LE_s is set to a minimum value of 30 W.m^{-2} so that one accounts for the small but non neglectable vapor flow reaching the surface (Boulet et al., 1997). The system is then solved for vegetation latent heat flux (LE_v). If LE_v is also negative, both LE_s and LE_v values are set to zero, whatever the value of T_{rad}. The system of equation can also be solved for T_s and T_v only if the efficiencies representing stress levels (dependent on surface soil moisture for the evaporation, and root zone soil moisture for the transpiration) are known. In that case the sole first four equations are solved. This prescribed mode allows computing all the fluxes in known limiting soil moisture levels (very dry, e.g. fully stressed, and wet enough, e.g. potential). It limits unrealistically high values of component fluxes, latent heat flux values above the potential rates or sensible heat flux values above that of a non evaporating surface.

Some of the model parameters were remotely sensed data while others were taken from the bibliography or measured *in situ*.

Remotely sensed data fed into SPARSE are: land surface temperature (LST), surface emissivity (ε) and viewing angle (ϕ) (MOD11A1/ MYD11A1 for Terra and Aqua, respectively), NDVI (MOD13A2/MYD13A2 for Terra and Aqua, respectively) and albedo (α) (MCD43B1, MCD43B2, MCD43B3). These data were acquired for the study period (1^{st} September 2012 to 30^{th} June 2015) at the resolution of the MODIS sensor at 1 km, embarked on board of the satellites Terra (overpass time around 10:30 local solar time) and Aqua (overpass time around 13:30 local solar time).

MODIS data provided in sinusoidal projection was reprojected in UTM using the MODIS Reprojection Tool (MRT). Then the sub-images of 10 km× 8 km over the study zone (Figure 1) were extracted. Since the MODIS pixels in our study area are considered to include the same land use (mainly arboriculture with some annual crops), the footprint of the MODIS pixel resulting from the variation in the size of the ground area that is detected (variation in the view zenith angles) as well as to the MODIS gridding process (Peng et al., 2015) were not reconstructed. The daily MODIS LST and viewing angle, 8-day MODIS albedo, and 16-day MODIS NDVI contain some missing or unreliable data; hence, days with missing data in MODIS pixels regarding the scintillometer footprint were excluded. Temporal interpolation of albedo and NDVI data were done to get daily remote sensing data.

A single equation (Clevers, 1989) was used to compute remotely sensed leaf area index (LAI) from the NDVI of all crops in the study area:

$$LAI = -\frac{1}{k} ln\left(\frac{NDVI_{\infty} - NDVI}{NDVI_{\infty} - NDVI_{soil}}\right) \quad (16)$$

The calibration of this relationship was done over the Yaqui irrigated perimeter (Mexico) during the 2007-2008 growing season using hemispherical LAI measured in all the studied fields (Chirouze et al., 2014). Calibration results gave the asymptotical values of NDVI, $NDVI_{\infty} = 0.97$ and $NDVI_{soil} = 0.05$, as well as the extinction factor k1.13. As this relationship was calibrated over a heterogeneous land surface but on herbaceous vegetation only, its relevance for trees was checked. For that purpose, clump-LAI measurements on an olive tree, as well as allometric measurements (mean distance between trees and mean crown size done using Pleiades satellite data (Mougenot et al., 2014;Touhami, 2013)) were obtained. We checked that the pixels with tree dominant cover show LAI values close to what was expected (of the order of 0.3 to 0.4 given the interrow distance of 12 m on average).

A grid of the vegetation height (z_v) was also necessary as input in the SPARSE model; for herbaceous crops, vegetation height was interpolated with the help of NDVI time series between fixed minimum (0.05 m) and maximum (0.8 m) values, while for trees, the roughness length (z_{om}) was linked to the allometric measurements (mentioned before) and computed as a function of canopy area index, drag coefficient and canopy height using the drag partition approach proposed by (Raupach, 1994) for tall sparse vegetative environments. Then, since SPARSE deals with vegetation height and not roughness length, the same simple rule of the thumb as the one used in SPARSE was used to reconstruct z_v for the tree cover types ($z_v = z_{om}/0.13$). In a final step, to get spatial vegetation height, z_v was averaged over the MODIS pixels.

In situ parameters used in SPARSE were mainly meteorological data: incoming solar radiation (Rg), incoming atmospheric radiation (R_{atm}), air temperature (Ta), air humidity (Ha) and wind speed (u).

No calibration was performed on the model parameters shown in Table 1.

Table 1. SPARSE parameters

	Definition	**Value**	**Data Sources**
Remote sensing parameters			
NDVI	Normalized Difference Vegetation Index		Satellite imagery
Trad (K)	Radiative surface temperature (K)		Satellite imagery
α	Albedo		Satellite imagery
ε	Emissivity		Satellite imagery
Φ (rad)	View zenith angle		Satellite imagery
Meteorological parameters			
R_g ($W.m^{-2}$)	Incoming solar radiation		In situ data
R_{atm} ($W.m^{-2}$)	Incoming atmospheric radiation		In situ data
T_a (K)	Air temperature at reference level		In situ data
RH_a (%)	Air relative humidity		In situ data
u_a ($m.s^{-1}$)	Horizontal wind speed at reference level		In situ data
Fixed parameters			
z_a (m)	Atmospheric forcing height	2.32	In situ data
z_v (m)	Vegetation height		Derived from land cover
β_{pot}	Evapotranspiration efficiency in full potential conditions	1.000	
β_{stress}	Evapotranspiration efficiency in fully stressed conditions	0.001	
r_{stmin} ($s.m^{-1}$)	Minimum stomatal resistance	100	Bibliography (Boulet et al., 2015)
w (m)	Leaf width	0.05	Bibliography (Braud et al., 1995)
ε_v	Vegetation emissivity	0.98	Bibliography (Braud et al., 1995)
α_v	Vegetation albedo	0.25	Estimation
Constants			
ρ_{cp} ($J.kg^{-1}.K^{-1}$)	Product of air density and specific heat	1170	Bibliography (Braud et al., 1995)
σ ($W.\ m^{-2}.k^{4}$)	Stefan–Boltzmann constant	$5.66.\ 10^{-8}$	Bibliography (Braud et al., 1995)
γ ($Pa.K^{-1}$)	Psychrometric constant	0.66	Bibliography (Braud et al., 1995)
$z_{om,s}$(m)	Equivalent roughness length of the underlying bare soil in the absence of vegetation	5.10^{-3}	Bibliography (Braud et al., 1995)
n_{SW}	Coefficient in r_{av} (Aerodynamic resistance between the vegetation and the aerodynamic level)	2.5	Bibliography (Boulet et al., 2015)
ξ	Ratio between soil heat flux G and available net radiation on the bare soil Rn_s	0.4	Bibliography (Braud et al., 1995)

SPARSE was run for the 10 km × 8 km sub-image at the time of Terra-MODIS and Aqua-MODIS overpass. Then, instantaneous modelled fluxes were multiplied by the nearest half hourly footprint to the satellite overpass time, in order to get fluxes corresponding to the upwind area ($H\_SPARSE_{t\text{-}FP}$, $LE\_SPARSE_{t\text{-}FP}$ and $AE\_SPARSE_{t\text{-}FP}$). In a subsequent step, SPARSE model was run at a half hourly time step using the half hourly meteorological measurements and assuming that the remote-sensed MODIS data are invariant during the same day.

4.2 Reconstruction of daily modelled ET from instantaneous latent heat flux

Daily ET is usually required for applications in hydrology or agronomy for instance, whereas most SEB methods provide a single instantaneous latent heat flux because the energy budget is only computed at the satellite overpass time (Delogu et al., 2012). In order to scale daily ET from one instantaneous measurement, various methods relying on the preservation, during the day, of the ratio of the latent heat flux to a scale factor having known diurnal evolution, have been developed. The global solar incoming radiation Rg, the net radiation Rn, the available energy or a maximum ET rate are generally used as scale factors. Chávez et al. (2008) , Colaizzi et al. (2005) and Van Niel et al. (2011) tested several extrapolation methods to estimate daily ET. The most common methods use as scaling factors the available energy or the potential ET. The first method assumes a constant diurnal evaporative fraction (EF) which is defined as the ratio of the latent heat flux (LE) to the available energy (Rn-G) at the land surface (Eq. (17)). The second one assumes a constant stress factor (SF) which is defined as the complementary part to 1 of the ratio between the simulated (actual conditions) and the potential (theoretical value for an unstressed surface i.e. potential ET) latent heat fluxes (LEpot (Eq. (18)). Potential ET is usually computed using a reference calculation such as the FAO-56 (Allen et al., 1998) method or derived from a surface energy balance model (e.g. Lhommel, 1997)

$$EF = \frac{LE}{Rn-G} \tag{17}$$

$$SF = 1 - \frac{LE}{LEpot} \tag{18}$$

Besides, daily ET can also be estimated using the residual method, after computing the daily H, Rn and G (same approach as for the XLAS derived LE detailed in Sect. 3.3).

All daily ET estimates were done for the 10 km × 8 km sub-image ($\mathrm{LE\_SPARSE_{day}}$) and then were weighted by the corresponding daily footprint to get the daily ET of the upwind area ($\mathrm{LE\_SPARSE_{day-FP}}$).

4.2.1 Evaporative Fraction method

Under clear sky days, EF self preservation was revised by several studies. Hoedjes et al. (2008) showed that EF is almost constant during daytime under dry conditions whereas it follows a concave-up shape under wet conditions. Hence, EF depends strongly on soil moisture as well as canopy fraction cover, but, it is nearly unrelated to solar radiation and wind speed, as shown by Gentine et al. (2007).

Consequently, the daily ET total (i.e. $\mathrm{LE\_SPARSE_{day}}$) can be expressed as the product of the instantaneous estimate of EF at the satellite overpass time and the daily available energy $\mathrm{AE\_SPARSE_{day}}$:

$$\boldsymbol{LE\_\mathrm{SPARSE}_{day}} = \boldsymbol{EF} \times \mathbf{AE\_SPARSE}_{\boldsymbol{day}} \tag{19}$$

Daily cumulative available energy $\mathrm{AE\_SPARSE_{day}}$ was computed from instantaneous available energy ($\mathrm{AE\_SPARSE_{t}}$) at the two satellite overpass times using the same approach detailed in Sect. 3.3.2 (Eq. (13) and Eq. (14)). Instantaneous estimates of Rn and G with the SPARSE model were used.

4.2.2 Stress Factor (SF) method

Assuming that the stress factor (SF) is constant during the day, the daily ET ($\mathrm{LE\_SPARSE_{day}}$) can be expressed as the product of the instantaneous estimate of SF at the satellite overpass time and the daily potential evapotranspiration $\mathrm{LEpot_{day}}$:

$$\boldsymbol{LE\_\mathrm{SPARSE}_{day}} = (\mathbf{1} - \boldsymbol{SF}) \times \boldsymbol{LEpot_{day}} \tag{20}$$

$LEpot_{day}$ was calculated as the sum of the half hourly modelled latent heat fluxes at potential conditions. The SF method is more complex than the EF method since inputs for the SF method have to be computed from a potential evapotranspiration model while inputs used for EF method can be derived from remote sensing.

4.2.3 Residual method

Daily modelled latent heat flux ($LE\_residual\_SPARSE_{day}$) was estimated as a residual term of the surface energy budget using daily modelled sensible heat flux (H_SPARSE_{day}) and available energy (AE_SPARSE_{day}) totals as shown in Eq. (21).

$$\mathbf{LE\_residual\_SPARSE_{day} = AE\_SPARSE_{day} - H\_SPARSE_{day}} \tag{21}$$

H_SPARSE_{day} was computed from modelled instantaneous H (H_SPARSE_t) following the same extrapolation method used for the available energy (see Sect. 3.3.2):

$$\mathrm{H\_SPARSE}_{\mathrm{day}_{\mathrm{Aqua}}} = \mathrm{a'}_{\mathrm{Terra}} \times \mathrm{Rg}_{\mathrm{day}} \frac{\mathrm{H\_SPARSE}_{\mathrm{t}_{\mathrm{Aqua}}}}{\mathrm{Rg}_{\mathrm{t}}} \mp \mathrm{b'}_{\mathrm{Terra}} \tag{22}$$

$$\mathrm{H\_SPARSE}_{\mathrm{day}_{\mathrm{Terra}}} = \mathrm{a'}_{\mathrm{Aqua}} \times \mathrm{Rg}_{\mathrm{day}} \frac{\mathrm{H\_SPARSE}_{\mathrm{t}_{\mathrm{Terra}}}}{\mathrm{Rg}_{\mathrm{t}}} + \mathrm{b'}_{\mathrm{Aqua}} \tag{23}$$

where Rg_t and Rg_{day} are respectively the instantaneous and daily global incoming solar radiation.

5 Water stress estimates

Water stress estimation is crucial to deduct the root zone soil moisture level using remote sensing data, (Hain et al., 2009). Water stress results in a drop of actual evaporation below the potential rate. Its intensity is usually represented by a stress factor (SF) as defined in Sect. 4.2, ranging between 0 (unstressed surface) and 1 (fully stressed surface).

Values of SF at the time of Terra and Aqua overpass (SF_{mod}) have been computed from potential LE generated with the SPARSE model in prescribed conditions ($\beta s = \beta v = 1$). It is thus possible to relate SF_{mod} to a combination of radiative temperatures as follows:

$$SF_{mod} = 1 - \frac{LE}{LE_{pot}} = \frac{LST - Trad_{pot}}{Trad_{stress} - Trad_{pot}} \tag{24}$$

where LE and LE_{pot} are the simulated latent heat fluxes in actual and potential conditions, respectively, and $Trad_{stress}$ and $Trad_{pot}$ are simulated radiative temperature in actual and potential conditions, respectively; and LST is the MODIS land surface temperature.

Furthermore, surface water stress factor derived from XLAS measurement, named SF_{obs}, at the time of Terra and Aqua overpass was computed as follows (Su, 2002):

$$SF_{obs} = \frac{H\_XLAS_t - H_{pot}}{H_{stress} - H_{pot}} \tag{25}$$

where H_{stress} and H_{pot} are the simulated sensible heat flux in actual and potential conditions, respectively; and H_XLAS_t is the XLAS sensible heat flux at the satellite overpass time.

6 Results and discussion

6.1 Reconstruction of daily available energy and sensible heat flux

For the sake of validation, daily AE computed from half hourly in situ data measured in the Ben Salem flux station (from November 2012 to June 2013) were compared to daily AE_{day} estimated from instantaneous AE_t using the scaling method based on Rg at both Terra-MODIS and Aqua-MODIS time overpass (see Sect. 3.3.2). This comparison was achieved only for clear sky days for which MODIS images can be acquired and remote sensing data used to compute AE are available. In order to select clear sky days, the ratio of the incoming solar radiation Rg to the theoretical clear sky radiation Rso as proposed by the FAO-56 method (Allen et al., 1998) was computed. A day was defined as clear if the measured Rg is higher than 85 % of the theoretical clear sky radiation at the satellite overpass time (Delogu et al., 2012).

An overestimation of about 15% is found between measured and estimated daily available energy (Figure 3); and the coefficients a_{Terra}, b_{Terra}, a_{Aqua} and b_{Aqua} (Table 2) were applied to remove this bias.

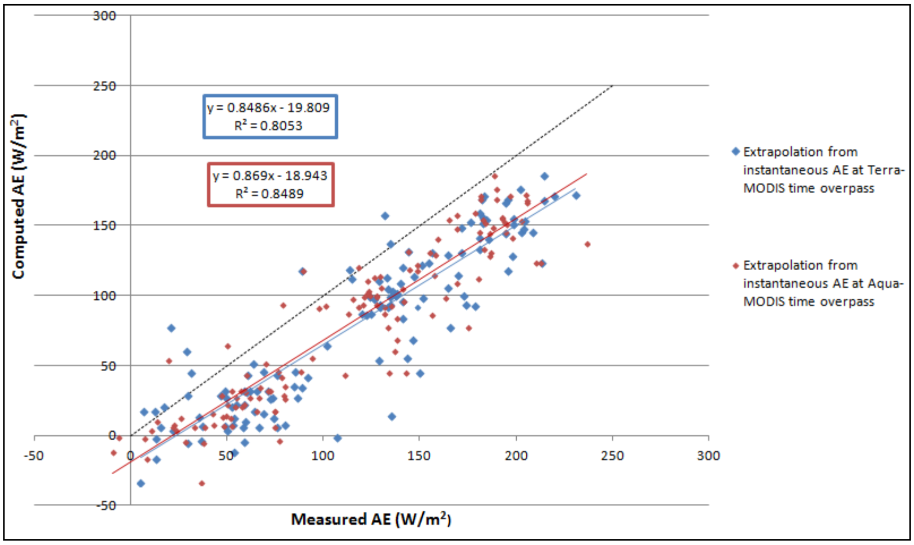

Figure 3: Comparison of daily AE observed at Ben Salem flux station (2012-2013) and daily AE estimated using the scaling method based on Rg.

Using the same approach, figure 4 shows the comparison of daily H observed at Ben Salem flux station (2012-2013) and daily H estimated using the scaling method based on Rg. The coefficients a'_{Terra}, b'_{Terra}, a'_{Aqua} and b'_{Aqua} (Table 2) were applied to remove the bias between measured and estimated daily H.

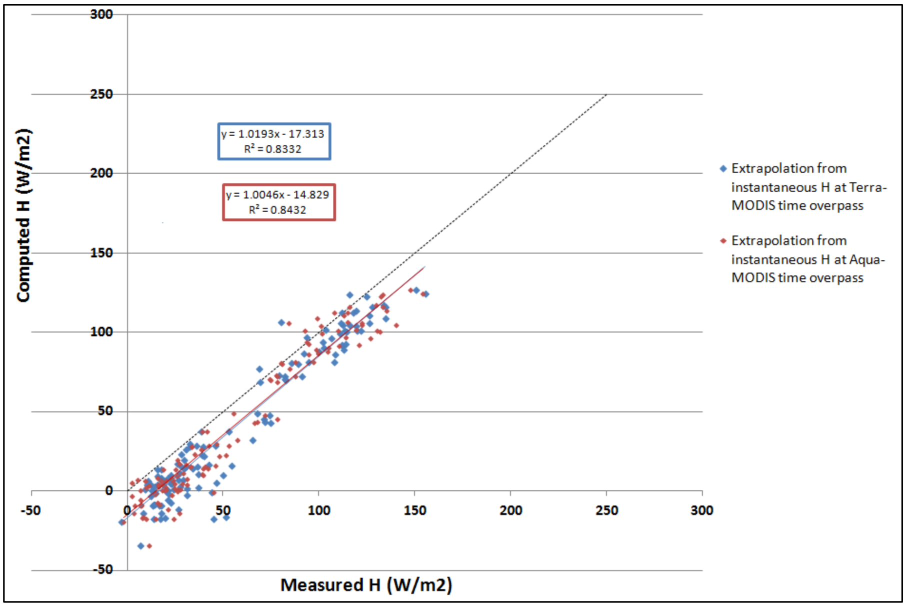

Figure 4: Comparison of daily H observed at Ben Salem flux station (2012-2013) and daily H estimated using the scaling method based on Rg.

Table 2: Corrected parameterizations of AE and H

Available energy (AE)	Terra	a_{Terra}	0.85
		b_{Terra}	-19.81
	Aqua	a_{Aqua}	0.87
		b_{Aqua}	-18.94
Sensible heat flux (H)	Terra	a'_{Terra}	1.02
		b'_{Terra}	-17.31
	Aqua	a'_{Aqua}	1.00
		b'_{Aqua}	-14.83

6.2 XLAS and model derived instantaneous sensible heat fluxes

Our primary focus is the comparison between scintillometer measurements and the modelled sensible heat fluxes computed using the Terra and Aqua remotely sensed data. The scintillometer H at the time of the two satellites overpass (H_XLAS$_t$) are interpolated from the half hourly H measurements and are shown in figure 5. Heat flux determination was possible for typically about 87% of the daytime measurements during the summer, availability of XLAS heat flux values was less during the cold season due to poor visibility and/or stable stratification.

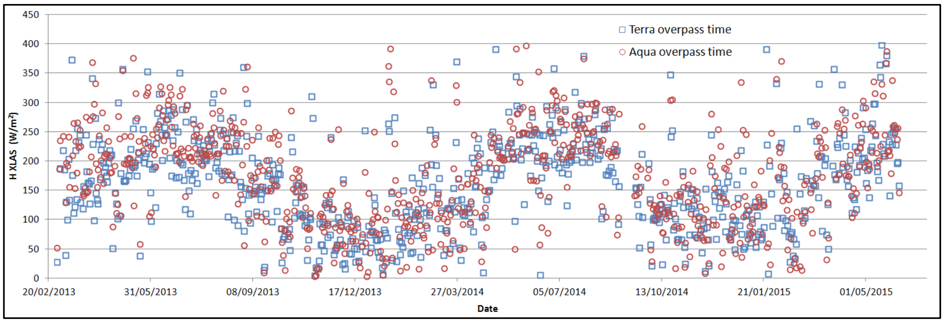

Figure 5: Time series of XLAS measured sensible heat flux (H) at the time of Terra and Aqua overpass

By convolving the XLAS footprint with the SPARSE derived H, we were able to compare the modelled values ($H\_SPARSE_{t\text{-}FP}$) with the XLAS measurements (H_XLAS_t). Therefore, due to XLAS and remote sensing data availability, we got 175 dots and 118 dots for Terra and Aqua respectively. As example, we present this comparison for two days of special interest, DOY 2013-083 and DOY 2014-185 (Figure 6). The colored area shows the modelled flux and the contours shows the surface source area contributing to 95% of the scintillometer measurements. The DOY 2013-083 corresponds to a large footprint with a south wind while the DOY 2014-185 corresponds to smaller upwind area with a north wind. Generally, a little number of MODIS pixels brings a high contribution to the signal; among them two are hot pixels in which the land use is mainly arboriculture.

Prediction performance is assessed using two widely-used indicators: the root-mean-square error (RMSE) and the coefficient of determination (R^2). Results for the sensible heat flux are illustrated in figure 7 and show good agreement between modelled and measured H at the time of satellites overpass. This is illustrated by linear regressions of $H\_SPARSE_{t\text{-}FP} = 1.065\ H\_XLAS_t - 14.788$ ($R^2 = 0.6$; RMSE = 57.89 $W.m^{-2}$) and $H\_SPARSE_{t\text{-}FP} = 1.12\ H\_XLAS_t - 10.57$ ($R^2 = 0.63$; RMSE = 53.85 $W.m^{-2}$) for Terra and Aqua, respectively. This result is of great interest considering that the SPARSE model was run with no prior calibration. Whereas there are several studies dealing with large aperture scintillometer (LAS) data whose measurements are compared to modelled fluxes, in the few studies dealing with extra large aperture scintillometer (XLAS) data, the comparison is generally done with Eddy Covariance station measurements (Kohsiek et al., 2002; Moene et al., 2006). Indeed, our results are in agreement with those found by Marx et al.(2008) who compared LAS-derived and satellite-derived H (SEBAL was applied with NOAA-AVHRR images providing maps of surface energy fluxes at a 1 km × 1 km spatial resolution), and found that modelled H is underestimated with a RMSE of 39 $W.m^{-2}$ for the site Tamale and 104 $W.m^{-2}$ for the site Ejura. Moreover, Watts et al.(2000) compared the satellite (AVHRR radiometer) estimates of H to those from LAS over a semi-arid grassland in northwest Mexico during the summer of 1997. They found RMSE values of 31 $W.m^{-2}$ and 43 $W.m^{-2}$ for LAS path lengths of 300 m and 600 m respectively and showed that LAS measurements are less good than those derived from a 3D sonic anemometer. They also suggested longer LAS path length (greater than 1.1 km) since the LAS is rather insensitive to the surface near the receiver and emitter.

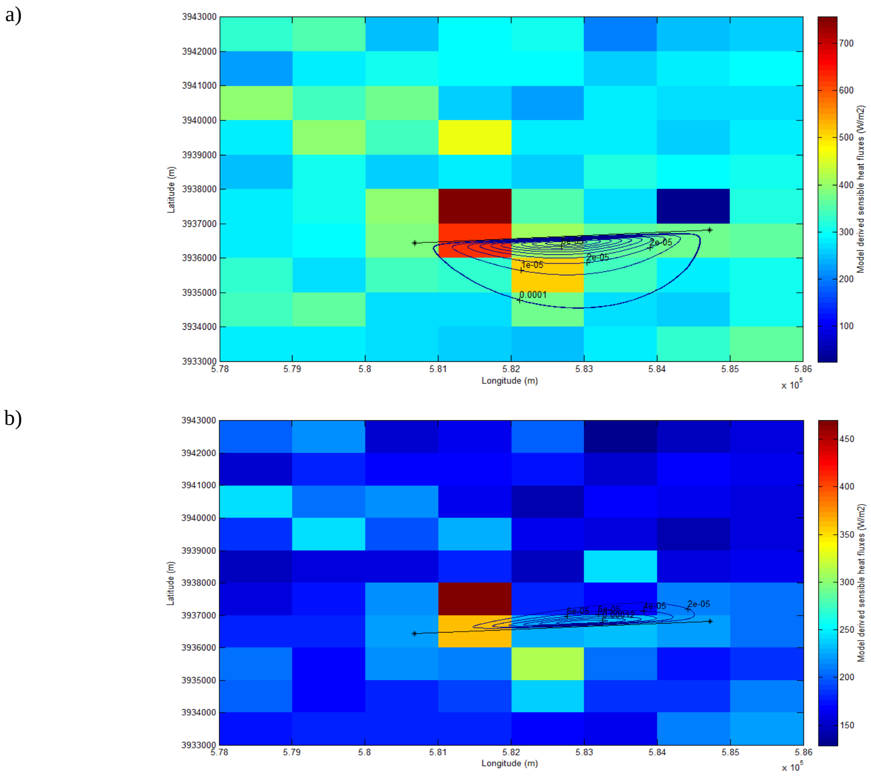

Figure 6: Model derived sensible heat fluxes and footprints for (a) DOY 2013-083 at Aqua time overpass and (b) DOY 2014-185 at Terra time overpass

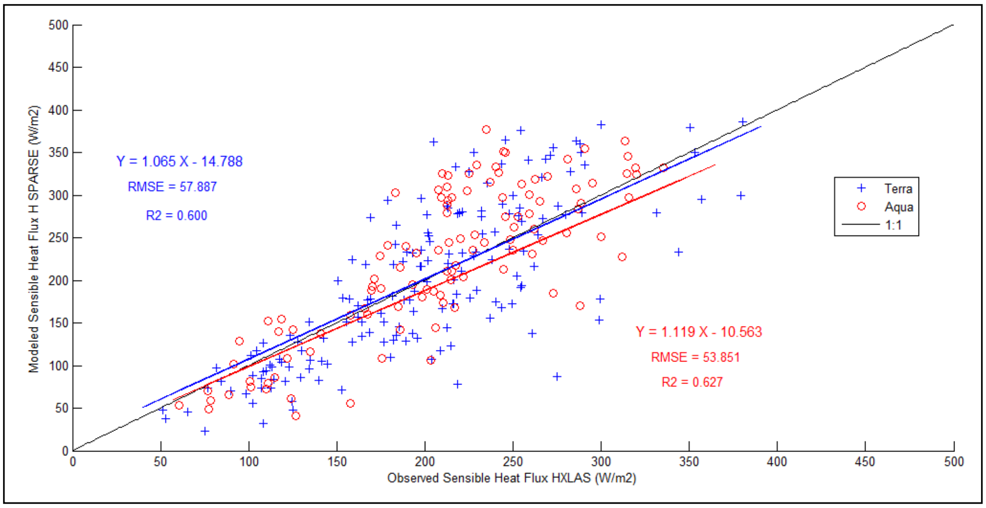

Figure 7: Modelled vs. observed sensible heat fluxes at Terra and Aqua time overpass

6.3 XLAS and model derived instantaneous latent heat fluxes

In a subsequent step, SPARSE derived LE (LE_SPARSE$_{t\text{-}FP}$) was compared to observed LE (LE_residual_XLAS$_{t\text{-}FP}$). Results are illustrated in figure 8 showing a good agreement between modelled and observed LE. However, these results are less good than for the H results, as shown by the linear regressions: LE_SPARSE$_{t\text{-}FP}$ =0.94 LE_residual_XLAS$_{t\text{-}FP}$ + 12.47 (RMSE = 47.20 W.m^{-2}) and LE_SPARSE$_{t\text{-}FP}$ = 0.85 LE_residual_XLAS$_{t\text{-}FP}$ +11.51 (RMSE = 43.20 W.m^{-2}) for Terra and Aqua respectively, with an overall R^2 of 0.55 for both satellites. We note a greater scatter for latent heat flux than for the sensible heat flux (Figure 7), which can be explained by the fact that LE is here a residual term affected by errors in both estimated AE and H. Despite this moderate discrepancy, the good agreement between both approaches indicates that the methodology adopted in SPARSE for estimating H and AE using MODIS imagery is appropriate for modeling latent heat fluxes.

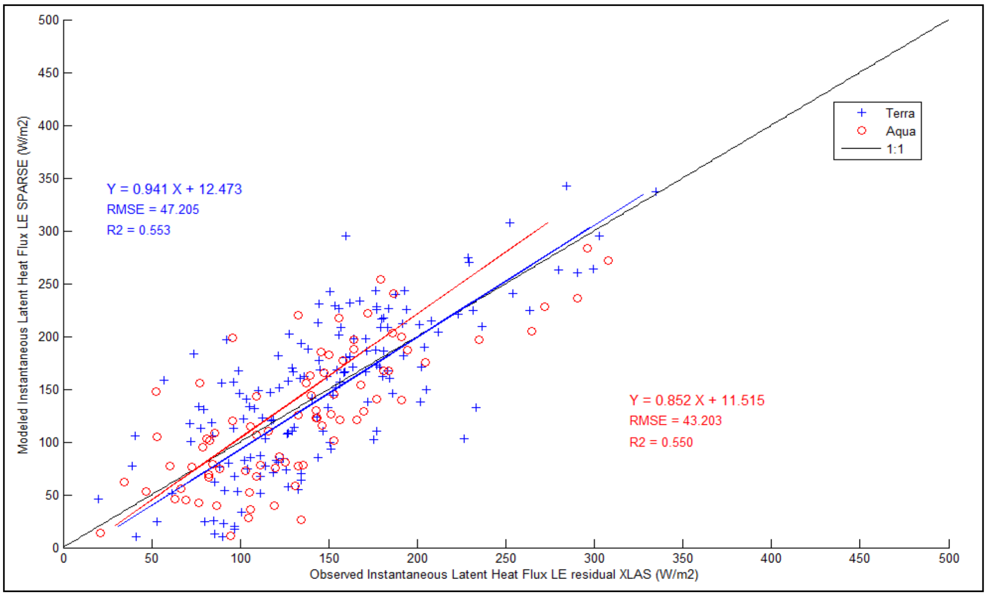

Figure 8: Modelled Vs. Observed latent heat fluxes at Terra and Aqua time overpass

6.4 Water stress

The scattered values of the Stress Factor as shown in figure 9 are consistent with previous studies such as Boulet et al. (2015). SEB retrieval of stress is limited by the scale mismatch between the instantaneous estimate of the surface temperature during the satellite overpass (which can be influenced by high frequency turbulence) and the aggregated values of other forcing data which are derived from half hourly averages (Lagouarde et al., 2013; Lagouarde et al., 2015). However, general tendencies are well reproduced, with most points located within a 0.2 confidence interval (illustrated by dotted lines along the 1:1 line) as found by Boulet et al. (2015) at plot scale, which is encouraging in a perspective of assimilating ET or SF in a water balance model for example. Moreover, it is noted that results include small LE and LE$_{pot}$ values having the same order of magnitude as the measurement uncertainty itself. Most outliers having greater water stress (~1) correspond to high evaporation from bare soil since the dominant land use in the study area is arboriculture, but also, this could be due to saturation of scintillation which led to an underestimation of H XLAS measurements as pointed by Frehlich and Ochs (1990) and Kohsiek et al. (2002).

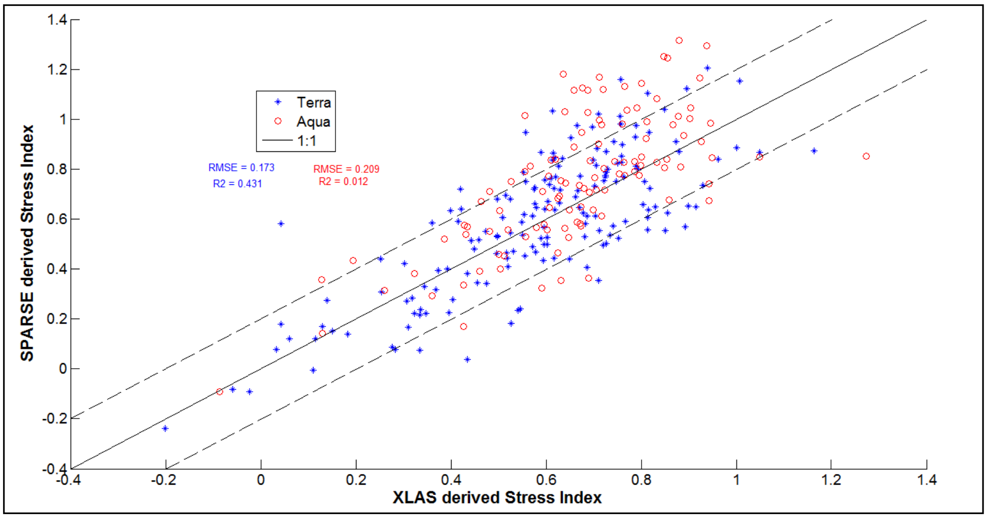

Figure 9: Modelled Vs. XLAS derived stress index SF at Terra and Aqua time overpass

Modelled and observed stress index at Terra and Aqua time overpass show a consistent evolution with daily rainfall (Figure 10), although the modelled stress show a greater dispersion than the observed one. During a rainy episode (or an eventual irrigation period), the surface temperature decreases towards the unstressed surface temperature, thus marking an unstressed state, and SF tends to 0. Conversely, after a long dry down, the water stress appears and the surface temperature increases towards the equilibrium surface temperature computed by SPARSE under stressed conditions, and SF tends towards 1. Besides, it is noted that modelled stress indexes computed on the basis of Aqua MODIS's LST are often greater than those computed used Terra MODIS's LST due to higher LST (higher global solar radiation) at the time of Terra overpass (around midday).

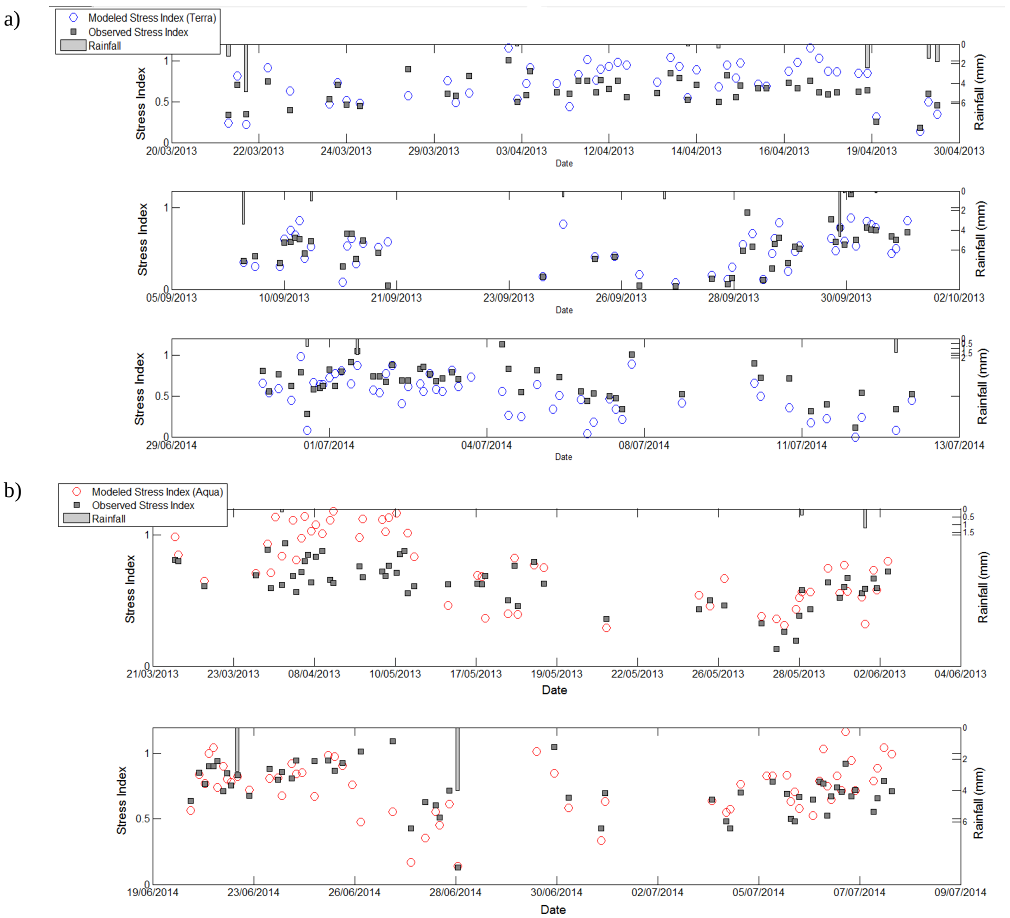

Figure 10: Modelled and observed Stress index evolution at (a) Terra and (b) Aqua time overpass compared to daily rainfall

6.5 XLAS and model derived daily latent heat fluxes

Daily observed ET, i.e. LE_residual_XLAS$_{day\text{-}FP}$, was computed using the residual method; hence, six estimates of the daily observed ET were obtained by combining the two satellite passes data and three methods to compute G and thus AE (see Sect. 3.3). Only the residual method was used to estimate daily observed ET for two reasons; on the first hand, to reduce the computations approach since, already, three methods to compute AE have been tested and on the other hand, the application of the EF method was not possible because we do not dispose of spatialized measured potential evapotranspiration (only point potential evapotranspiration data at the Ben Salem meteorological station are available). From daily observed ET estimates, minimum and maximum ET were selected for each day and minimum and maximum daily ET time series were interpolated between successive days based on the self preservation of the ratio of the available energy (AE) to the global incoming radiation Rg as scale factor (Figure 11).

In addition, three methods were used to compute SPARSE daily ET for the Terra and Aqua overpasses (see Sect. 4.2), providing six estimates of the daily modelled ET. For each day average ET was plotted (260 days) with error bars figuring minimum and maximum values, along with precipitation to understand the rainfall impact on the ET evolution (Figure 11).

Despite the uncertainty in reconstructing the daily ET from instantaneous ET, overall results show a good agreement between XLAS derived and SPARSE derived ET values with similar seasonal dynamics. Daily observed and modelled ET over the whole study period were both in the range of 0-4 mm mm.day^{-1} which is consistent with the land use present in the XLAS path: mainly trees with a considerable fraction of bare soil. As expected, ET rates decrease significantly during dry periods (summers) and increase immediately after rainfall events. The rainfall peaks that occurred on 3rd September 2013 (about 10mm), 6th October 2013 (about 20 mm), 15th March 2014 (about 100 mm) and 22nd April 2014 (about 25 mm) are followed by well-reproduced drydown (soil drying) events.

At seasonal scale, we note a good agreement between modelled and observed daily ET for the 2013-2014 and 2014-2015 seasons, especially when vegetation cover was more developed: from March to July 2014 and from March to Mai 2015; these periods correspond to cereals vegetation peak in some plots (March-April) and to market gardening crops (e.g. tomato, water melon, pepper…) cultivated generally from spring to the beginning of autumn in the interrow area of trees plots, which is a common farming practice in the Kairouan plain. However, the 2012-2013 season was dry compared with the two other ones, and less accurate results were obtained. Some points with little to null ET were recorded from May to July 2013 which can be explained by the very dry conditions and scattered vegetation cover with a considerable amount of bare soil. Lower ET values are generally recorder in autumn (October and November) which correspond to evapotranspiration from trees only, since the latest summer crops (market gardening crops) have been already harvested and the winter crops (mainly cereals) are not yet sown.

Moreover, it can be seen that occasionally SPARSE model overestimated ET. As example, three dates can be selected in August 2013 (15th, 25th and 29th August 2013) for which modelled ET were 3.30 mm, 3.80 mm and 2.80 mm while maximum observed ET were 2.0 mm, 2.40 mm and 1.20 mm, respectively; broader amplitude between modelled (4.00 mm) and observed ET (1.40 mm) was also recorded on the 18th of May 2013. SPARSE also overestimates ET throughout ten days in August 2014 with an average difference of 1.1 mm and a maximum difference of 1.60 mm recorded in 23rd August 2014. These discrepancies are always recorded under wet conditions (minimum stress factor) which show the difficulty in representing accurately the conditions close to the potential ET. This might be related to the theoretical limit of the model for low vegetation stress especially when coupled with low evaporation efficiencies (i.e. dry soil surface) as already reported by Boulet et al. (2015) for senescent vegetation. Average difference between SPARSE and XLAS derived LE estimates when both are available indicate that SPARSE can predict evapotranspiration with accuracies approaching 5% of that of the XLAS.

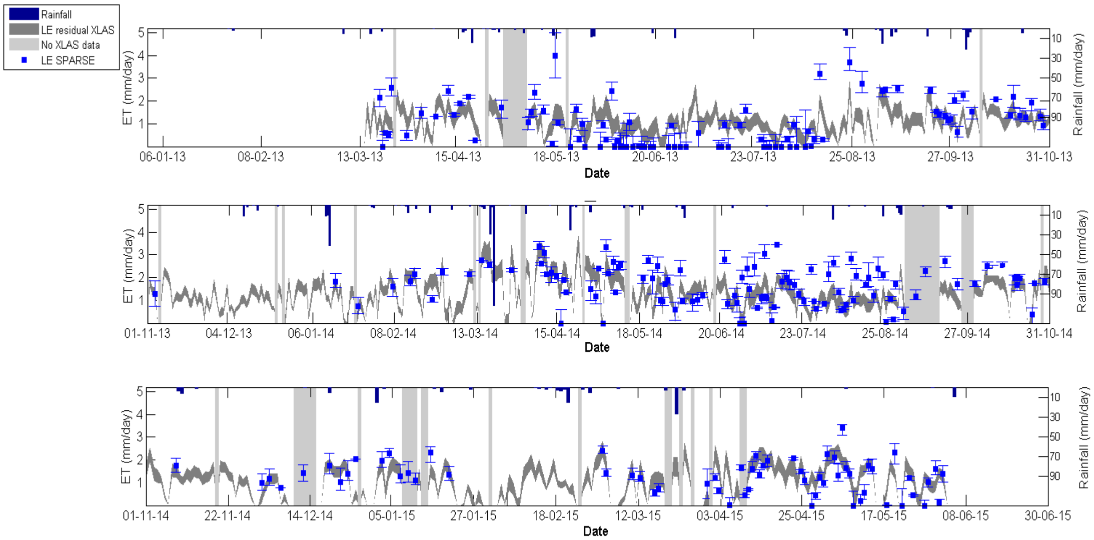

Figure 11: Modelled vs. observed daily latent heat fluxes. Light grey bars show gaps in XLAS data.

7 Conclusions

This study evaluated the performances of the SPARSE model forced by MODIS remote sensing products in an operational context (no model calibration) to estimate instantaneous and daily evapotranspiration. The validation protocol was based on an unprecedented dataset with an extra large aperture scintillometer. Indeed, up to our knowledge, this is the first work based on XLAS measurements acquired during more than 2 years, as compared to three months in previous works (Kohsiek et al., 2002;Moene et al., 2006). The estimates of the sensible heat flux derived from the SPARSE model are in close agreement with those obtained from the XLAS. These results indicate that the XLAS can be fruitfully used to validate large-scale sensible heat flux derived from remote sensing data (and residual latent heat flux), in particular for the results obtained at the satellite overpass time, providing a feasible alternative to local micrometeorological techniques for measuring the sensible heat flux and validating satellite-derived estimates (i.e. eddy correlation). Furthermore, the extrapolation from instantaneous to daily evapotranspiration is less obvious and three methods were tested based on the stress index, the evaporative fraction and the residual approach. The daily latent heat fluxes derived from the XLAS agreed rather well with those modelled using SPARSE model, which shows the potential of the SPARSE model in water consumption monitoring over heterogeneous landscape in semi-arid conditions, and especially to locate areas most affected by water stress. Even though overall results are encouraging, further work is needed to better valorize the XLAS dataset and improve results by i) being most efficient in the SPARSE model application using calibrated input data specific to our study area, especially input parameters to which the model is particularly sensitive such as the mean leaf width and the minimum stomatal resistance and ii) taking into account the heterogeneity of the 1km MODIS pixel by applying MODIS footprint, which is determined by the sensor's observation geometry.

Finally, in a future work, we plan to take advantage of the complementarities between the Soil Water Balance and Surface Energy Balance approaches (i.e. continuous but uncertain estimates using SWB due to poor soil water content control on one hand and sensitivity of SEB to the actual water stress on the other hand) to implement an assimilation scheme of the remotely sensed surface temperature into SVAT models. In fact, in order to provide further information about distributed soil water status over the studied areas, the TIR-derived evapotranspiration products could be assimilated directly either in SVAT or hydrological models.

Author contribution:

Sameh Saadi: data processing, data analysis and results interpretation.
Gilles Boulet: data analysis and results interpretation.
Malik Bahir: SPARSE inputs and XLAS data processing and analysis.
Aurore Brut: XLAS data processing and analysis.
Bernard Mougenot and Zohra Lili Chabaane: site management.
Pascal Fanise: site instrumentation.
Vincent Simonneaux and Zohra Lili-Chabaane contributed with ideas and discussions.

Competing interests:

The authors declare that they have no conflict of interest.

Acknowledgements

The authors are thankful to the GDAs of Ben Salem I and Ben Salem II which enabled the scintillometer set-up and access above the two water towers. Funding from the CNES/TOSCA program for the EVA2IRT project, from the MISTRALS/SICMED program for the ReSAMEd project, from the ORFEO/CNES Program for Pléiades images (© CNES 2012, Distribution Airbus DS, all rights reserved), and from the ANR/TRANSMED program for the AMETHYST project (ANR-12-TMED-0006-01) as well as the mobility support from PHC Maghreb program (N° 32592VE) are gratefully acknowledged,. This work has benefited also from the financial support of the ARTS program ("Allocations de recherche pour une thèse au Sud") of IRD (Institut de Recherche pour le Développement).

References

Allen, R., Irmak, A., Trezza, R., Hendrickx, J. M., Bastiaanssen, W., and Kjaersgaard, J.: Satellite-based ET estimation in agriculture using SEBAL and METRIC, Hydrological Processes, 25, 4011-4027, 2011.

Allen, R. G., Pereira, L. S., Raes, D., and Smith, M.: Crop evapotranspiration-Guidelines for computing crop water requirements-FAO Irrigation and drainage paper 56, FAO, Rome, 300, D05109, 1998.

Allen, R. G., Tasumi, M., and Trezza, R.: AIP Conf. Proc., 852, 127, 2005.

Allen, R. G., Tasumi, M., and Trezza, R.: J. Irrig. Drain. Eng., 133, 395, 2007.

Amri, R., Zribi, M., Lili-Chabaane, Z., Szczypta, C., Calvet, J. C., and Boulet, G.: FAO-56 dual model combined with multi-sensor remote sensing for regional evapotranspiration estimations, Remote Sensing, 6, 5387-5406, 2014.

Anderson, M. C., Kustas, W. P., Norman, J. M., Hain, C. R., Mecikalski, J. R., Schultz, L., González-Dugo, M. P., Cammalleri, C., d'Urso, G., Pimstein, A., and Gao, F.: Mapping daily evapotranspiration at field to continental scales using geostationary and polar orbiting satellite imagery, Hydrol. Earth Syst. Sci., 15, 223-239, 10.5194/hess-15-223-2011, 2011.

Andreas, E. L.: Atmospheric stability from scintillation measurements, Applied optics, 27, 2241-2246, 1988.

Bai, J., Liu, S., and Mao, D.: Area-averaged evapotranspiration fluxes measured from large aperture scintillometer in the Hai River basin, River Basin Research And Planning Approach, edited by: Zhang, H., Zhao, R., and Zhoa, H., Orient ACAD Forum, Marrickville, Australia, 2009, 331-340,

Bastiaanssen, W. G. M.: Regionalization of surface flux densities and moisture indicators in composite terrain; a remote sensing approach under clear skies in mediterranean climates, SC-DLO, Wageningen, 1995.

Bastiaanssen, W. G. M.: J. Irrig. Drain. Eng., 131, 85, 2005.

Bastiaanssen, W. G. M., Allen, R. G., Droogers, P., D'Urso, G., and Steduto, P.: Twenty-five years modeling irrigated and drained soils: State of the art, Agricultural Water Management, 92, 111-125, http://dx.doi.org/10.1016/j.agwat.2007.05.013, 2007.

Bisht, G., Venturini, V., Islam, S., and Jiang, L.: Estimation of the net radiation using MODIS (Moderate Resolution Imaging Spectroradiometer) data for clear sky days, Remote Sensing of Environment, 97, 52-67, https://doi.org/10.1016/j.rse.2005.03.014, 2005.

Boulet, G., Braud, I., and Vauclin, M.: Study of the mechanisms of evaporation under arid conditions using a detailed model of the soil–atmosphere continuum. Application to the EFEDA I experiment, Journal of Hydrology, 193, 114-141, https://doi.org/10.1016/S0022-1694(96)03148-4, 1997.

Boulet, G., Chehbouni, A., Gentine, P., Duchemin, B., Ezzahar, J., and Hadria, R.: Monitoring water stress using time series of observed to unstressed surface temperature difference, Agricultural and Forest Meteorology, 146, 159-172, https://doi.org/10.1016/j.agrformet.2007.05.012, 2007.

Boulet, G., Mougenot, B., Lhomme, J. P., Fanise, P., Lili-Chabaane, Z., Olioso, A., Bahir, M., Rivalland, V., Jarlan, L., Merlin, O., Coudert, B., Er-Raki, S., and Lagouarde, J. P.: The SPARSE model for the prediction of water stress and evapotranspiration components from thermal infra-red data and its evaluation over irrigated and rainfed wheat, Hydrol. Earth Syst. Sci., 19, 4653-4672, 10.5194/hess-19-4653-2015, 2015.

Bounoua, L., Zhang, P., Thome, K., Masek, J., Safia, A., Imhoff, M. L., and Wolfe, R. E.: Mapping Biophysical Parameters for Land Surface Modeling over the Continental US Using MODIS and Landsat, Dataset Papers in Science, 2015, 11, 10.1155/2015/564279, 2015.

Braud, I., Dantas-Antonino, A. C., Vauclin, M., Thony, J. L., and Ruelle, P.: A simple soil-plant-atmosphere transfer model (SiSPAT) development and field verification, Journal of Hydrology, 166, 213-250, http://dx.doi.org/10.1016/0022-1694(94)05085-C, 1995.

Brunsell, N. A., Ham, J. M., and Arnold, K. A.: Validating remotely sensed land surface fluxes in heterogeneous terrain with large aperture scintillometry, International Journal of Remote Sensing, 32, 6295-6314, 10.1080/01431161.2010.508058, 2011.

Burba, G. G., Verma, S. B., and Kim, J.: Surface energy fluxes of Phragmites australis in a prairie wetland, Agricultural and Forest Meteorology, 94, 31-51, https://doi.org/10.1016/S0168-1923(99)00007-6, 1999.

Calera, A., Campos, I., Osann, A., D'Urso, G., and Menenti, M.: Remote Sensing for Crop Water Management: From ET Modelling to Services for the End Users, Sensors, 17, 1104, 2017.

Chávez, J., Neale, C. M. U., Hipps, L. E., Prueger, J. H., and Kustas, W. P.: Comparing Aircraft-Based Remotely Sensed Energy Balance Fluxes with Eddy Covariance Tower Data Using Heat Flux Source Area Functions, Journal of Hydrometeorology, 6, 923-940, 10.1175/jhm467.1, 2005.

Chávez, J. L., Neale, C. M. U., Prueger, J. H., and Kustas, W. P.: Daily evapotranspiration estimates from extrapolating instantaneous airborne remote sensing ET values, Irrigation Science, 27, 67-81, 10.1007/s00271-008-0122-3, 2008.

Chehbouni, A., Watts, C., Lagouarde, J. P., Kerr, Y. H., Rodriguez, J. C., Bonnefond, J. M., Santiago, F., Dedieu, G., Goodrich, D. C., and Unkrich, C.: Estimation of heat and momentum fluxes over complex terrain using a large aperture scintillometer, Agricultural and Forest Meteorology, 105, 215-226, https://doi.org/10.1016/S0168-1923(00)00187-8, 2000.

Chirouze, J., Boulet, G., Jarlan, L., Fieuzal, R., Rodriguez, J. C., Ezzahar, J., Er-Raki, S., Bigeard, G., Merlin, O., Garatuza-Payan, J., Watts, C., and Chehbouni, G.: Intercomparison of four remote-sensing-based energy balance methods to retrieve surface evapotranspiration and water stress of irrigated fields in semi-arid climate, Hydrol. Earth Syst. Sci., 18, 1165-1188, 10.5194/hess-18-1165-2014, 2014.

Choudhury, B., and Monteith, J.: A four-layer model for the heat budget of homogeneous land surfaces, Quarterly Journal of the Royal Meteorological Society, 114, 373-398, 1988.

Choudhury, B. J., Idso, S. B., and Reginato, R. J.: Analysis of an empirical model for soil heat flux under a growing wheat crop for estimating evaporation by an infrared-temperature based energy balance equation, Agricultural and Forest Meteorology, 39, 283-297, http://dx.doi.org/10.1016/0168-1923(87)90021-9, 1987.

Clevers, J. G. P. W.: Application of a weighted infrared-red vegetation index for estimating leaf Area Index by Correcting for Soil Moisture, Remote Sensing of Environment, 29, 25-37, http://dx.doi.org/10.1016/0034-4257(89)90076-X, 1989.

Colaizzi, P. D., Evett, S. R., Howell, T. A., and Tolk, J. A.: Comparison of Five Models to Scale Daily Evapotranspiration from One-Time-of-Day Measurements, 10.13031/2013.18885, 2005.

Cragoa, R., and Brutsaert, W.: Daytime evaporation and the self-preservation of the evaporative fraction and the Bowen ratio, Journal of Hydrology, 178, 241-255, http://dx.doi.org/10.1016/0022-1694(95)02803-X, 1996.

Danelichen, V. H. d. M., Biudes, M. S., Souza, M. C., Machado, N. G., Silva, B. B. d., and Nogueira, J. d. S.: Estimation of soil heat flux in a neotropical Wetland region using remote sensing techniques, Revista Brasileira de Meteorologia, 29, 469-482, 2014.

De Bruin, H. A. R., and Wang, J.: Scintillometry: a review. Researchgate, 2017.

Delogu, E., Boulet, G., Olioso, A., Coudert, B., Chirouze, J., Ceschia, E., Le Dantec, V., Marloie, O., Chehbouni, G., and Lagouarde, J. P.: Reconstruction of temporal variations of evapotranspiration using instantaneous estimates at the time of satellite overpass, Hydrol. Earth Syst. Sci., 16, 2995-3010, 10.5194/hess-16-2995-2012, 2012.

Ezzahar, J., Chehbouni, A., Hoedjes, J., Ramier, D., Boulain, N., Boubkraoui, S., Cappelaere, B., Descroix, L., Mougenot, B., and Timouk, F.: Combining scintillometer measurements and an aggregation scheme to estimate area-averaged latent heat flux during the AMMA experiment, Journal of Hydrology, 375, 217-226, http://dx.doi.org/10.1016/j.jhydrol.2009.01.010, 2009.

Feddes, R. A., Kowalik, P. J., and Zaradny, H.: Simulation of Field Water Use and Crop Yield, Wiley, 1978.

Frehlich, R. G., and Ochs, G. R.: Effects of saturation on the optical scintillometer, Applied optics, 29, 548-553, 1990.

Gentine, P., Entekhabi, D., Chehbouni, A., Boulet, G., and Duchemin, B.: Analysis of evaporative fraction diurnal behaviour, Agricultural and Forest Meteorology, 143, 13-29, https://doi.org/10.1016/j.agrformet.2006.11.002, 2007.

Giorgi, F., and Avissar, R.: Representation of heterogeneity effects in earth system modeling: Experience from land surface modeling, Reviews of Geophysics, 35, 413-437, 1997.

Glenn, E. P., Huete, A. R., Nagler, P. L., Hirschboeck, K. K., and Brown, P.: Integrating remote sensing and ground methods to estimate evapotranspiration, Critical Reviews in Plant Sciences, 26, 139-168, 2007.

Green, A. E., and Hayashi, Y.: Use of the scintillometer technique over a rice paddy, Journal of Agricultural Meteorology, 54, 225-234, 1998.

Hain, C. R., Mecikalski, J. R., and Anderson, M. C.: Retrieval of an Available Water-Based Soil Moisture Proxy from Thermal Infrared Remote Sensing. Part I: Methodology and Validation, Journal of Hydrometeorology, 10, 665-683, 10.1175/2008jhm1024.1, 2009.

Hartogensis, O. K., Watts, C. J., Rodriguez, J.-C., and Bruin, H. A. R. D.: Derivation of an Effective Height for Scintillometers: La Poza Experiment in Northwest Mexico, Journal of Hydrometeorology, 4, 915-928, 10.1175/1525-7541(2003)004<0915:doaehf>2.0.co;2, 2003.

Hemakumara, H. M., Chandrapala, L., and Moene, A. F.: Evapotranspiration fluxes over mixed vegetation areas measured from large aperture scintillometer, Agricultural Water Management, 58, 109-122, http://doi.org/10.1016/S0378-3774(02)00131-2, 2003.

Hill, R., Clifford, S. F., and Lawrence, R. S.: Refractive-index and absorption fluctuations in the infrared caused by temperature, humidity, and pressure fluctuations, JOSA, 70, 1192-1205, 1980.

Hoedjes, J. C. B., Chehbouni, A., Jacob, F., Ezzahar, J., and Boulet, G.: Deriving daily evapotranspiration from remotely sensed instantaneous evaporative fraction over olive orchard in semi-arid Morocco, Journal of Hydrology, 354, 53-64, https://doi.org/10.1016/j.jhydrol.2008.02.016, 2008.

Horst, T., and Weil, J.: Footprint estimation for scalar flux measurements in the atmospheric surface layer, Boundary-Layer Meteorology, 59, 279-296, 1992.

Hunink, J., Eekhout, J., Vente, J., Contreras, S., Droogers, P., and Baille, A.: Hydrological Modelling using Satellite-Based Crop Coefficients: A Comparison of Methods at the Basin Scale, Remote Sensing, 9, 174, 2017.

Jackson, R. D., Moran, M. S., Gay, L. W., and Raymond, L. H.: Evaluating evaporation from field crops using airborne radiometry and ground-based meteorological data, Irrigation Science, 8, 81-90, 10.1007/bf00259473, 1987.

Jacobs, J. M., Myers, D. A., Anderson, M. C., and Diak, G. R.: GOES surface insolation to estimate wetlands evapotranspiration, Journal of Hydrology, 266, 53-65, https://doi.org/10.1016/S0022-1694(02)00117-8, 2002.

Kalma, J. D., McVicar, T. R., and McCabe, M. F.: Estimating land surface evaporation: A review of methods using remotely sensed surface temperature data, Surveys in Geophysics, 29, 421-469, 2008.

Kohsiek, W., Meijninger, W. M. L., Moene, A. F., Heusinkveld, B. G., Hartogensis, O. K., Hillen, W. C. A. M., and De Bruin, H. A. R.: An Extra Large Aperture Scintillometer For Long Range Applications, Boundary-Layer Meteorology, 105, 119-127, 10.1023/a:1019600908144, 2002.

Kohsiek, W., Meijninger, W. M. L., Debruin, H. A. R., and Beyrich, F.: Saturation of the Large Aperture Scintillometer, Boundary-Layer Meteorology, 121, 111-126, 10.1007/s10546-005-9031-7, 2006.

Kustas, W., and Anderson, M.: Advances in thermal infrared remote sensing for land surface modeling, Agricultural and Forest Meteorology, 149, 2071-2081, 2009.

Kustas, W. P., and Daughtry, C. S. T.: Estimation of the soil heat flux/net radiation ratio from spectral data, Agricultural and Forest Meteorology, 49, 205-223, http://dx.doi.org/10.1016/0168-1923(90)90033-3, 1990.

Kustas, W. P., Daughtry, C. S. T., and Van Oevelen, P. J.: Analytical treatment of the relationships between soil heat flux/net radiation ratio and vegetation indices, Remote Sensing of Environment, 46, 319-330, http://dx.doi.org/10.1016/0034-4257(93)90052-Y, 1993.

Kustas, W. P., and Norman, J. M.: Evaluation of soil and vegetation heat flux predictions using a simple two-source model with radiometric temperatures for partial canopy cover, Agricultural and Forest Meteorology, 94, 13-29, https://doi.org/10.1016/S0168-1923(99)00005-2, 1999.

Lagouarde, J.-P., Bonnefond, J.-M., Kerr, Y. H., McAneney, K. J., and Irvine, M.: Integrated Sensible Heat Flux Measurements of a Two-Surface Composite Landscape using Scintillometry, Boundary-Layer Meteorology, 105, 5-35, 10.1023/a:1019631428921, 2002a.

Lagouarde, J.-P., Jacob, F., Gu, X. F., Olioso, A., Bonnefond, J.-M., Kerr, Y., Mcaneney, K. J., and Irvine, M.: Spatialization of sensible heat flux over a heterogeneous landscape, Agronomie-Sciences des Productions Vegetales et de l'Environnement, 22, 627-634, 2002b.

Lagouarde, J.-P., Bach, M., Sobrino, J. A., Boulet, G., Briottet, X., Cherchali, S., Coudert, B., Dadou, I., Dedieu, G., and Gamet, P.: The MISTIGRI thermal infrared project: scientific objectives and mission specifications, International journal of remote sensing, 34, 3437-3466, 2013.

Lagouarde, J.-P., Irvine, M., and Dupont, S.: Atmospheric turbulence induced errors on measurements of surface temperature from space, Remote Sensing of Environment, 168, 40-53, https://doi.org/10.1016/j.rse.2015.06.018, 2015.

Leclerc, M. Y., and Thurtell, G. W.: Footprint prediction of scalar fluxes using a Markovian analysis, Boundary-Layer Meteorology, 52, 247-258, 10.1007/bf00122089, 1990.

Leduc, C., Calvez, R., Beji, R., Nazoumou, Y., Lacombe, G., and Aouadi, C.: Evolution de la ressource en eau dans la vallée du Merguellil (Tunisie centrale), Séminaire sur la modernisation de l'agriculture irriguée, 2004, 10 p.,

Lhommel, J.-P.: Towards a rational definition of potential evaporation, Hydrology and Earth System Sciences Discussions, 1, 257-264, 1997.

Li, Z.-L., Tang, R., Wan, Z., Bi, Y., Zhou, C., Tang, B., Yan, G., and Zhang, X.: A review of current methodologies for regional evapotranspiration estimation from remotely sensed data, Sensors, 9, 3801-3853, 2009.

Liou, Y.-A., and Kar, S.: Evapotranspiration Estimation with Remote Sensing and Various Surface Energy Balance Algorithms—A Review, Energies, 7, 2821, 2014.

Ma, Y., Su, Z., Li, Z., Koike, T., and Menenti, M.: Determination of regional net radiation and soil heat flux over a heterogeneous landscape of the Tibetan Plateau, Hydrological Processes, 16, 2963-2971, 2002.

Marx, A., Kunstmann, H., Schüttemeyer, D., and Moene, A. F.: Uncertainty analysis for satellite derived sensible heat fluxes and scintillometer measurements over Savannah environment and comparison to mesoscale meteorological simulation results, Agricultural and Forest Meteorology, 148, 656-667, https://doi.org/10.1016/j.agrformet.2007.11.009, 2008.

Mauser, W., and Schädlich, S.: Modelling the spatial distribution of evapotranspiration on different scales using remote sensing data, Journal of Hydrology, 212, 250-267, 1998.

Meijninger, W. M. L., Hartogensis, O. K., Kohsiek, W., Hoedjes, J. C. B., Zuurbier, R. M., and De Bruin, H. A. R.: Determination of Area-Averaged Sensible Heat Fluxes with a Large Aperture Scintillometer over a Heterogeneous Surface – Flevoland Field Experiment, Boundary-Layer Meteorology, 105, 37-62, 10.1023/a:1019647732027, 2002.

Minacapilli, M., and Ciraolo, G.: Evaluating actual evapotranspiration by means of multi-platform remote sensing data: a case study in Sicily, 2007.

Minacapilli, M., Agnese, C., Blanda, F., Cammalleri, C., Ciraolo, G., D'Urso, G., Iovino, M., Pumo, D., Provenzano, G., and Rallo, G.: Estimation of actual evapotranspiration of Mediterranean perennial crops by means of remote-sensing based surface energy balance models, Hydrology and Earth System Sciences, 13, 1061-1074, 2009.

Mira, M., Olioso, A., Gallego-Elvira, B., Courault, D., Garrigues, S., Marloie, O., Hagolle, O., Guillevic, P., and Boulet, G.: Uncertainty assessment of surface net radiation derived from Landsat images, Remote Sensing of Environment, 175, 251-270, 2016.

Moene, A. F., Meijninger, W., Kohsiek, W., Gioli, B., Miglietta, F., and Bosveld, F.: Validation of fluxes of an extra large aperture scintillometer at Cabauw using sky arrow aircraft flux measurements, Proceedings of 17th symposium on boundary layers and turbulence. American Meteorological Society, San Diego, CA, 2006, 22-25,

Mougenot, B., Touhami, N., Lili Chabaane, Z., Boulet, G., Simonneaux, V., and Zribi, M.: Trees detection for water resources management in irrigated and rainfed arid and semi-arid agricultural areas, Pléiades Days, Toulouse, April 1-3, 2014, 2014.

Mutziger, A. J., Burt, C. M., Howes, D. J., and Allen, R. G.: Comparison of measured and FAO-56 modeled evaporation from bare soil, Journal of irrigation and drainage engineering, 131, 59-72, 2005.

Nichols, W. E., and Cuenca, R. H.: Evaluation of the evaporative fraction for parameterization of the surface energy balance, Water Resources Research, 29, 3681-3690, 10.1029/93wr01958, 1993.

Odi-Lara, M., Campos, I., Neale, C., Ortega-Farías, S., Poblete-Echeverría, C., Balbontín, C., and Calera, A.: Estimating Evapotranspiration of an Apple Orchard Using a Remote Sensing-Based Soil Water Balance, Remote Sensing, 8, 253, 2016.

Oki, T., and Kanae, S.: Global Hydrological Cycles and World Water Resources, Science, 313, 1068-1072, 10.1126/science.1128845, 2006.

Payero, J. O., Neale, C. M. U., and Wright, J. L.: Estimating Diurnal Variation of Soil Heat Flux for Alfalfa and Grass, Proceedings of the 2001 ASAE Annual Meeting Sacramento, California, 10.13031/2013.5546, 2001.

Peng, J., Liu, Q., Wang, L., Liu, Q., Fan, W., Lu, M., and Wen, J.: Characterizing the Pixel Footprint of Satellite Albedo Products Derived from MODIS Reflectance in the Heihe River Basin, China, Remote Sensing, 7, 6886, 2015.

Pereira, L. S., Oweis, T., and Zairi, A.: Irrigation management under water scarcity, Agricultural water management, 57, 175-206, 2002.

Poussin, J. C., Imache, A., Beji, R., Le Grusse, P., and Benmihoub, A.: Exploring regional irrigation water demand using typologies of farms and production units: An example from Tunisia, Agricultural Water Management, 95, 973-983, https://doi.org/10.1016/j.agwat.2008.04.001, 2008.

Pradeleix, L., Roux, P., Bouarfa, S., Jaouani, B., Lili-Chabaane, Z., and Bellon-Maurel, V.: Environmental Impacts of Contrasted Groundwater Pumping Systems Assessed by Life Cycle Assessment Methodology: Contribution to the Water–Energy Nexus Study, Irrigation and Drainage, 64, 124-138, 2015.

Raupach, M. R.: Simplified expressions for vegetation roughness length and zero-plane displacement as functions of canopy height and area index, Boundary-Layer Meteorology, 71, 211-216, 10.1007/bf00709229, 1994.

Saadi, S., Simonneaux, V., Boulet, G., Raimbault, B., Mougenot, B., Fanise, P., Ayari, H., and Lili-Chabaane, Z.: Monitoring Irrigation Consumption Using High Resolution NDVI Image Time Series: Calibration and Validation in the Kairouan Plain (Tunisia), Remote Sensing, 7, 13005, 2015.

Samain, B., Simons, G. W., Voogt, M. P., Defloor, W., Bink, N.-J., and Pauwels, V.: Consistency between hydrological model, large aperture scintillometer and remote sensing based evapotranspiration estimates for a heterogeneous catchment, Hydrology and Earth System Sciences, 16, 2095-2107, 2012.

Schmid, H. P.: Footprint modeling for vegetation atmosphere exchange studies: a review and perspective, Agricultural and Forest Meteorology, 113, 159-183, https://doi.org/10.1016/S0168-1923(02)00107-7, 2002.

Shuttleworth, W. J., Gurney, R. J., Hsu, A. Y., and Ormsby, J. P.: FIFE: The Variation in Energy Partition at Surface Flux Sites, 1989.

Shuttleworth, W. J., and Gurney, R. J.: The theoretical relationship between foliage temperature and canopy resistance in sparse crops, Quarterly Journal of the Royal Meteorological Society, 116, 497-519, 1990.

Solignac, P. A., Brut, A., Selves, J. L., Béteille, J. P., Gastellu-Etchegorry, J. P., Keravec, P., Béziat, P., and Ceschia, E.: Uncertainty analysis of computational methods for deriving sensible heat flux values from scintillometer measurements, Atmos. Meas. Tech., 2, 741-753, 10.5194/amt-2-741-2009, 2009.

Su, Z.: The Surface Energy Balance System (SEBS) for estimation of turbulent heat fluxes, Hydrology and Earth System Sciences Discussions, 6, 85-100, 2002.

Torres, E. A., and Calera, A.: Bare soil evaporation under high evaporation demand: a proposed modification to the FAO-56 model, Hydrological Sciences Journal–Journal des Sciences Hydrologiques, 55, 303-315, 2010.

Touhami, N.: Détection des arbres par imagerie Très Haute Résolution Spatiale sur la plaine de Kairouan Engineer, Institut National Agronomqiue de Tunisie, Tunis, 78 pp., 2013.

Tucker, C. J.: A comparison of satellite sensor bands for vegetation monitoring, 1978.

Twine, T. E., Kustas, W., Norman, J., Cook, D., Houser, P., Meyers, T., Prueger, J., Starks, P., and Wesely, M.: Correcting eddy-covariance flux underestimates over a grassland, Agricultural and Forest Meteorology, 103, 279-300, 2000.

Van Niel, T. G., McVicar, T. R., Roderick, M. L., van Dijk, A. I. J. M., Renzullo, L. J., and van Gorsel, E.: Correcting for systematic error in satellite-derived latent heat flux due to assumptions in temporal scaling: Assessment from flux tower observations, Journal of Hydrology, 409, 140-148, https://doi.org/10.1016/j.jhydrol.2011.08.011, 2011.

Wang, T.-i., Ochs, G. R., and Clifford, S. F.: A saturation-resistant optical scintillometer to measure Cn2†, Journal of the Optical Society of America, 68, 334-338, 10.1364/josa.68.000334, 1978.

Watts, C. J., Chehbouni, A., Rodriguez, J. C., Kerr, Y. H., Hartogensis, O., and de Bruin, H. A. R.: Comparison of sensible heat flux estimates using AVHRR with scintillometer measurements over semi-arid grassland in northwest Mexico, Agricultural and Forest Meteorology, 105, 81-89, http://doi.org/10.1016/S0168-1923(00)00188-X, 2000.

Xie, Y., Sha, Z., and Yu, M.: Remote sensing imagery in vegetation mapping: a review, Journal of Plant Ecology, 1, 9-23, 2008.

Zribi, M., Chahbi, A., Shabou, M., Lili-Chabaane, Z., Duchemin, B., Baghdadi, N., Amri, R., and Chehbouni, A.: Soil surface moisture estimation over a semi-arid region using ENVISAT ASAR radar data for soil evaporation evaluation, Hydrology and Earth System Sciences Discussions, 15, 345-358, 2011.